Structure Annotation and Quantification of Wheat Seed Oxidized Lipids by High-Resolution LC-MS/MS[1][CC-BY]

David Riewe,[2,3] Janine Wiebach,[2] and Thomas Altmann

Leibniz Institute of Plant Genetics and Crop Plant Research, 06466 Gatersleben, Germany

ORCID IDs: 0000-0002-9095-5518 (D.R.); 0000-0002-7416-9859 (J.W.); 0000-0002-3759-360X (T.A.).

Lipid oxidation is a process ubiquitous in life, but the direct and comprehensive analysis of oxidized lipids has been limited by available analytical methods. We applied high-resolution liquid chromatography-mass spectrometry (LC-MS) and tandem mass spectrometry (MS/MS) to quantify oxidized lipids (glycerides, fatty acids, phospholipids, lysophospholipids, and galactolipids) and implemented a platform-independent high-throughput-amenable analysis pipeline for the high-confidence annotation and acyl composition analysis of oxidized lipids. Lipid contents of 90 different naturally aged wheat (*Triticum aestivum*) seed stocks were quantified in an untargeted high-resolution LC-MS experiment, resulting in 18,556 quantitative mass-to-charge ratio features. In a posthoc liquid chromatography-tandem mass spectrometry experiment, high-resolution MS/MS spectra (5 mD accuracy) were recorded for 8,957 out of 12,080 putatively monoisotopic features of the LC-MS data set. A total of 353 nonoxidized and 559 oxidized lipids with up to four additional oxygen atoms were annotated based on the accurate mass recordings (1.5 ppm tolerance) of the LC-MS data set and filtering procedures. MS/MS spectra available for 828 of these annotations were analyzed by translating experimentally known fragmentation rules of lipids into the fragmentation of oxidized lipids. This led to the identification of 259 nonoxidized and 365 oxidized lipids by both accurate mass and MS/MS spectra and to the determination of acyl compositions for 221 nonoxidized and 295 oxidized lipids. Analysis of 15-year aged wheat seeds revealed increased lipid oxidation and hydrolysis in seeds stored in ambient versus cold conditions.

Lipid oxidation is a process inevitably connected to life. Although essential for all respiring organisms, oxygen can form reactive species (ROS). The accumulation of these compounds leads to the phenomenon commonly referred to as oxidative stress in microbes and plant and animal tissues. ROS play a role in the attack against microbial pathogens by host cells (Imlay, 2013), time-dependent death of dormant seeds (Lee et al., 2010), human diseases (Coyle and Puttfarcken, 1993; Giugliano et al., 1996), in aging (Sohal and Weindruch, 1996; Sohal et al., 2002), and in signaling processes (Gilroy et al., 2016; Mignolet-Spruyt et al., 2016). The severity of individual cytotoxic effects of ROS is so far not clear. It is known that macromolecules with important cellular functions like DNA (Yakes and Van Houten, 1997) or proteins (Berlett and Stadtman, 1997) are oxidized, but lipid (per)oxidation is an autocatalytic process and, hence, potentially more devastating once triggered. Typically, lipid oxidation is estimated indirectly by measuring malondialdehyde (Stewart and Bewley, 1980; Goel and Sheoran, 2003; Chu et al., 2012), 4-hydroxy-2-nonenal (Perluigi et al., 2012; Spickett, 2013), autoluminescence (Birtic et al., 2011), or fluorescent lipid oxide reaction products (Morita et al., 2016), but these assays do not resolve the oxidation at the level of lipid classes or individual lipids.

Unlike oxidized fatty acids (FAs), oxidized lipids are hardly available commercially. Targeted liquid chromatography-mass spectrometry (LC-MS) analysis of oxidized lipids using authentic standards is not very common (Hui et al., 2010; Ravandi et al., 2014). Often, oxidized lipids are detected using tandem mass spectrometry (MS/MS), where the collision-induced products of precursor ions (PRs) are scanned for fragments or neutral losses (NLs) that correspond to oxidized acyl residues expected in oxidized lipids (Spickett and Pitt, 2015), and in some cases, higher resolution MS/MS spectra are provided to support the identification (Buseman et al., 2006; Vu et al., 2012).

High-resolution mass spectrometry (MS) allows for the quantification and detection of analytes based on their accurate mass. It has been applied in the analysis of known or expected nonoxidized lipids in biological samples in a growing number of studies for more than a decade now either by direct infusion (shotgun lipidomics; Ejsing et al., 2009; Schwudke et al., 2011) or in combination with liquid chromatography (Giavalisco et al., 2011; Hummel et al., 2011). For identification, the mass-to-charge ratio (*m/z*) values of an untargeted LC-MS or

[1] This work was supported by the Bundesanstalt fuer Landwirtschaft und Ernaehrung, Germany (project 04/13-14NZL).

[2] These authors contributed equally to the article.

[3] Address correspondence to dariewe@googlemail.com.

The author responsible for distribution of materials integral to the findings presented in this article in accordance with the policy described in the Instructions for Authors (www.plantphysiol.org) is: David Riewe (dariewe@googlemail.com).

D.R. initiated the study, analyzed samples, and wrote the article with the help of J.W. and T.A.; J.W. analyzed samples and developed the computational workflow with the help of D.R.; T.A. supervised and complemented the writing.

www.plantphysiol.org/cgi/doi/10.1104/pp.17.00470

direct-infusion MS experiment are matched against the *m/z* values of known lipids, preferably at low error tolerance (typically 1–10 ppm).

At present, the number of oxidized lipids represented by entries in databases like LIPID MAPS (www.lipidmaps.org) is low. Structures of only eight oxidized phosphatidylcholines (PCs; LIPID MAPS classifier GP2001), 15 oxidized phosphatidylethanolamines (PEs; GP2002), and three oxidized cardiolipins (GP2003) are currently available. The FA composition of these phospholipids (PLs) does not represent the situation in plant membrane lipids, where typically C16/C18 FAs dominate in lipid structures. LIPID MAPS contains a large number of oxidized hydroxy FAs (FA0105) with various lengths and numbers of double bonds and up to three hydroxy groups, but hydroperoxy FAs (FA0104, FA0200, and FA03) are only available with 18 or more C atoms. Oxo FAs (FA0106 and FA0200) lack C16 oxo FAs with double bonds, and epoxy FAs (FA0107 and FA0200) with 16 C atoms are not listed. Mixtures of these modifications also are listed. Oxidized galactolipids (GLs), triacylglycerols (TAGs), and diacylglycerols (DAGs) are currently not present in LIPID MAPS.

Due to their systematic structure, lipids also were annotated database independently by comparison of accurate *m/z* values in untargeted LC-MS data sets with assembled target lists containing several thousand lipids belonging to different classes. Each lipid class is represented by lipids differing in carbon length and number of double bonds in the FA/acyl (or alkyl) residues (Giavalisco et al., 2011). Very recently, Collins et al. (2016) extended this approach by adding one to four additional oxygen atoms to the lipids in such a list to annotate oxidized lipids in chemically (H_2O_2) oxidized cultures of the diatom *Phaeodactylum tricornutum*. Their annotation workflow resulted in the tentative annotation of 1,969 unique lipid sum formulae with up to four additional oxygen molecules, but in their conclusions, the authors suggest utilizing MS/MS data to improve annotation certainty by reducing likely false-positive annotations.

The acyl chain/head group composition of intact lipids can be determined from MS/MS spectra using various commercial (LipidView [www.absciex.com] and LipidSearch [www.thermo.com]) or open-source software tools (http://www.lipidmaps.org/tools/ms/ and LipidXplorer; Herzog et al., 2002), because the rules of fragmentation are well understood for the most relevant lipids (LipidBlast; Kind et al., 2013). But the availability of and knowledge regarding MS/MS spectra of oxidized lipids are quite scarce and restricted to single lipid species like TAGs (Zeb, 2012) and PLs (Spickett and Pitt, 2015) or to particular acyl residues like oxidized C18 and C16 FA esters (Vu et al., 2012). All in all, there has been a lack of suitable strategies to generate and annotate untargeted high-resolution MS/MS spectra of an untargeted quantitative high-resolution LC-MS experiment in order to quantify and identify as many oxidized lipids as possible from a set of samples.

The application of the above-mentioned indirect assays as proxies for lipid oxidation has suggested that this process plays a substantial role in the natural (and artificial) aging of seeds, leading to losses in the viability and germinability of plant seeds from different species needed for production, conservation, and breeding purposes (Stewart and Bewley, 1980; Goel and Sheoran, 2003; Chen et al., 2016). Long-term seed repositories like gene banks started decades of years ago to store seeds in cold conditions, after it was found that this would preserve their viability for a longer time than storage at ambient temperatures (Roberts, 1960; Ellis et al., 1982). The life-prolonging effect of cold storage is assumed to be based upon slowing down oxidative stress, but molecular evidence like corresponding patterns of oxidized lipids were not investigated.

Here, we present a two-step procedure for the quantification and structural annotation of oxidized lipids belonging to the major lipid classes occurring naturally in long-term stored wheat (*Triticum aestivum*) seeds. In the first step, we quantitatively analyzed 90 wheat seed extracts with putative differences in oxidized lipids using high-resolution LC-MS and annotated lipid sum formulae using accurate mass data and filtering algorithms. In the second step, we generated high-resolution MS/MS spectra of a large fraction of all putative monoisotopic peaks of the LC-MS data set using liquid chromatography-tandem mass spectrometry (LC-MS/MS). We then analyzed the MS/MS spectra to validate the mass-based annotations and to determine their acyl compositions. In this way, 624 sum formulae (predominantly oxidized lipids) were MS/MS validated, with structural determinations for 516 of them. The comparison of oxylipid profiles of ambient and cold-stored seeds revealed increased lipid oxidation and hydrolysis at ambient conditions.

RESULTS

LC-MS Analysis of Wheat Seeds

Long-term stored wheat seeds were chosen as a model system to study lipid oxidation because lipid oxidation has been linked previously with seed viability (Lee et al., 2010; Colville et al., 2012; Chen et al., 2016). The wheat seed lipidome is not dominated by TAGs, as is the case for oilseeds like rapeseeds (*Brassica napus*) or Arabidopsis (*Arabidopsis thaliana*). This allows measuring more diverse lipids in parallel within the dynamic range typical for mass spectrometers. Metabolically, an orthodox seed is expected to be relatively inert. Ninety wheat seed stocks from the German Federal Ex Situ Genebank differing in genotype, harvest time point, and storage conditions were chosen for analysis. Lipids were extracted from 50 pooled seeds per stock and analyzed using high-resolution LC-MS in both positive and negative mode. An example positive-mode base peak chromatogram is provided in Figure 1A. After the removal of background signals, the positive-mode

peaktable had 18,556 chromatographic *m/z* features (Supplemental Table S1) with 8,836 deconvoluted pseudospectra/base peaks, theoretically representing individual analytes. The negative mode peaktable (Supplemental Table S2) had 5,554 *m/z* features and 3,161 pseudospectra. For positive mode, the distribution of chromatographic features along retention time and *m/z* is displayed in Figure 1B.

Generation of an Oxylipid Target List

We followed the approach of Collins et al. (2016) to generate a target list that contains oxidized lipids from an established conventional lipid target list (Hummel et al., 2011; Szymanski et al., 2014; Pant et al., 2015) developed by Giavalisco et al. (2011). Among others, this list of 2,009 entries contains storage and membrane lipids and FAs classified according to acyl/alkyl chain length and number of double bonds. We applied minor changes and extended this list by adding up to four oxygen atoms to the sum formulae of all entries. The final oxylipid target list (OxyLTL; Supplemental Table S3) contained 11,185 entries.

Mass-Based Annotation of Oxidized Major Plant Lipids

All putative monoisotopic *m/z* features (not [M+X] in Supplemental Tables S1 and S2, Isotopes) were searched against the OxyLTL in multiple adduct variants (Supplemental Protocol S1). The final *m/z* tolerance was 1.5 ppm in positive mode after *m/z* correction (described below, but applied within a loop from this step

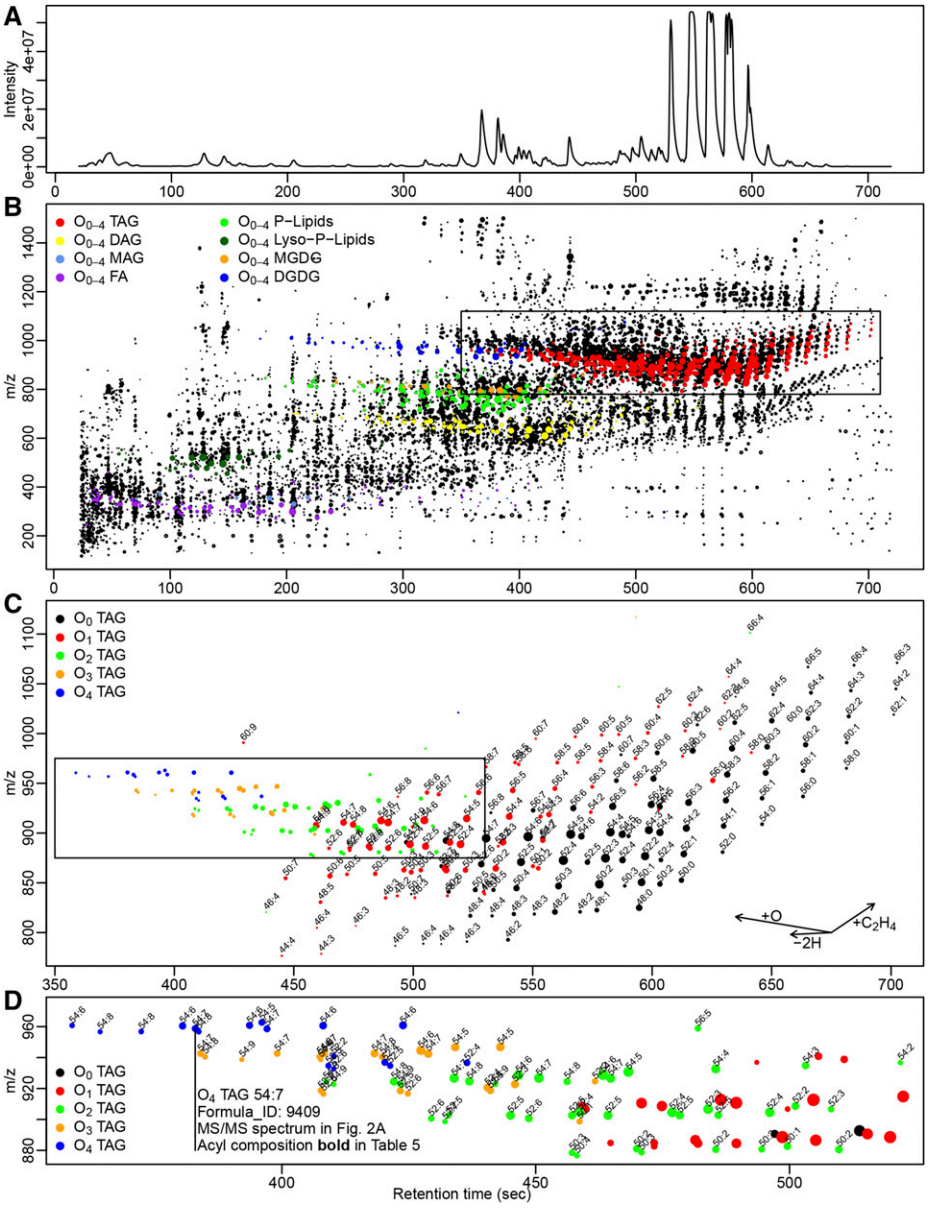

Figure 1. LC-MS analysis in positive mode. A, Example base peak chromatogram. B, Median retention time, *m/z*, and intensity (point size corresponds to $\log_{1000}$ transformed median ion count) of 18,556 chromatographic *m/z* features in 90 wheat seed stocks. Six hundred twenty-four identified lipids (with MS/MS validation) and 157 FAs (without MS/MS validation) are displayed in colors representing their lipid class. The boxed area is shown in higher magnification in C. C, O_1 (red) TAGs elute 40 s earlier than their cognate O_0 TAGs (black). The boxed area is shown in higher magnification in D. D, Higher oxidized TAGs occur as isomers with different retention times.

on). The data recorded in negative mode were annotated allowing for 5 ppm error, and where not *m/z* error corrected, they are used only for the validation of positive mode annotations (see "Bothmode Filter" below). In positive mode, this resulted in 5,050 annotations (Table I), and out of these, 3,201 belonged to the plant major lipid classes TAG, DAG, monoacylglycerol (MAG), PC, PE, phosphatidylglycerol (PG), phosphatidylinositol (PI), lysophosphatidylcholine (lysoPC), lysophosphatidylethanolamine (lysoPE), lysophosphatidylglycerol (lysoPG), lysophosphatidylinositol (lysoPI), monogalactosyldiacylglycerol (MGDG), and digalactosyldiacylglycerol (DGDG) in nonoxidized and oxidized form, which are the focus of this study.

Filtering Procedure for the Removal of False-Positive Annotations

For the annotations made in positive mode, filtering was applied to reduce the number of likely false-positive or redundant annotations. The applied filters are based on characteristics typical for chromatography, electrospray ionization, and isotope fidelity.

Isotope Filter

For sum formula annotations of monoisotopic peaks, the normalized isotope abundance was computed using enviPat (Loos et al., 2015) and compared with the observed normalized isotope pattern. The difference was expressed as root-mean-square-deviation in per mille (mSigma; Thiele et al., 2011). We found that isotope patterns calculated from median or individual peak areas of isotopic peaks often were imprecise, particularly for less intense signals. Instead, we extracted the normalized isotope pattern for every isotopic *m/z* feature at the apex scan in every chromatogram. mSigma values were calculated from the median normalized isotope pattern and from a linear modeled isotope pattern (Supplemental Table S1, mSigma by median and mSigma by lm). Only annotations with mSigma $<$ 60 (mass spectrometer specification is 50) in any of the two calculations were regarded as valid (Supplemental Table S1, Isotope filter = true). As an example, it disqualified diacylglyceryltrimethylhomoserine (DGTS) 36:4 to be the lipid represented by pseudospectrum 144 (Table II), and this procedure restricted the number of reliable annotations in the data set to 3,112 (Table I).

Bothmode Filter

If multiple sum formulae with different monoisotopic masses were assigned within one pseudospectrum, even if they were assigned to the same *m/z* (e.g. O_1 PC 36:4 and DGTS 36:4 but not O_1 PS [phosphatidylserine] 40:3 and O_3 PC 38:4; Table II), it was possible to identify a likely true positive annotation if one of these sum formulae also was detected in negative mode. For all annotations made for peaks in positive mode, we searched for peaks detected in negative mode that (1) coeluted within –4 to +1 s, (2) had an identical annotation, and (3) displayed a peak-to-peak Pearson correlation with $P < 0.05$. It can be expected that certain lipid species will be less efficiently determined due to a lower ionization in either of the two modes (e.g. TAGs in negative mode or FAs in positive mode). To account for this, the filter is applied only if cross-validation occurs within an *m/z* feature of a pseudospectrum. If, within a pseudospectrum, annotations also were identified in negative mode, these were marked true and all others were marked false (Supplemental Table S1, Bothmode filter). For instance, within pseudospectrum 144, only O_1 PC 36:4, O_1 PS 40:3, and O_3 PC 38:4 are cross-validated by identical annotations coinciding in negative mode; consequently, all other annotations within this pseudospectrum are disqualified. This procedure further restricted the number of valid annotations to 2,939 (Table I).

Adduct Filter

Some analytes form more than one adduct during electrospray ionization (e.g. $[M+H]^+$ and $[M+NH_4]^+$). To reduce the number of likely false annotations, we followed a modified approach of Collins et al. (2016) to enrich correct annotations. The dominant adduct of a lipid class and its oxides was defined as the most frequently found adduct for each class (without oxides) within our data set. The dominant adducts identified here for TAGs ($[M+NH_4]^+$), PEs ($[M+H]^+$), PCs ($[M+H]^+$),

Table I. *Number of annotations, pseudospectra, and base peak annotations after each filter step*

Filter Step	Annotations	Pseudospectra Annotations	Base Peak Annotations
All annotations (1.5 ppm)	5,050	2,612	3,322
Lipids of interest[a]	3,201	2,165	2,026
Isotope filter	3,112	2,123	1,987
Bothmode filter	2,939	2,110	1,957
Adduct filter	1,079	1,014	928
Retention filter	1,066	1,003	918
MSMS filter	624	607	556
MSMS filter (+FA)[b]	778	761	681

[a]TAG, DAG, MAG, PC, PE, PG, PI, lysoPC, lysoPE, lysoPG, lysoPI, MGDG, and DGDG. [b]FAs are not MS/MS validated.

Table II. *Example: filtering results in pseudospectrum 144 (Supplemental Table S1, pcgroup = 144)*

DGTS 36:4 is rejected by the isotope filter. O_1 PC 36:4, O_1 PS 40:3, and O_3 PC 38:4 are cross-identified in negative mode, thus disqualifying the other annotations. The adduct filter maintains O_1 PC 36:4 as $[M+H]^+$ adduct only; the $[M+Na]^+$ adduct is flagged false to avoid redundancy. None of the annotations violated the retention filter rules. O_1 PC 34:3, PC 36:5, and O_1 PC 36:4 were validated by their MS/MS spectra because all of them contain the PC-specific head group (Supplemental Table S6). Both O_1 PC 36:4 adducts ($[M+H]^+$ and $[M+Na]^+$) were confirmed by their MS/MS spectra. Only O_1 PC 36:4 $[M+H]^+$ passes all filters. Rt, Retention time (in seconds). "NA" in the "MS/MS Filter" column indicates either no available MS/MS spectrum or no applicable fragmentation rules for the lipid class.

Formula_ID	*m/z*	Rt	Sum Formula	Name	Adduct	Monoisotopic Mass	Error/ppm	Base Peak	Isotope Filter	Bothmode Filter	Adduct Filter	Retention Filter	MS/MS Filter	All Filters
1403	772.5484	298.57	$C_{42}H_{78}N_1O_9P_1$	O_1 PC 34:3	$[M+H]^+$	771.5414	0.14	False	True	False	False	True	True	False
5012	772.5484	298.57	$C_{44}H_{79}N_1O_7$	DGTS 34:3	$[M+K]^+$	733.5857	0.29	False	True	False	False	True	NA	False
637	780.5546	298.56	$C_{44}H_{78}N_1O_8P_1$	PC 36:5	$[M+H]^+$	779.5465	-1.28	False	True	False	False	True	True	False
1414	798.5641	298.56	$C_{44}H_{80}N_1O_9P_1$	O_1 PC 36:4	$[M+H]^+$	797.5571	0.11	True	True	True	True	True	True	True
5023	798.5641	298.56	$C_{46}H_{81}N_1O_7$	DGTS 36:4	$[M+K]^+$	759.6013	0.26	True	False	False	False	True	NA	False
3828	820.5461	298.56	$C_{44}H_{80}N_1O_9P_1$	O_1 PC 36:4	$[M+Na]^+$	797.5571	0.01	False	True	True	False	True	True	False
11190	902.5487	298.57	$C_{46}H_{84}N_1O_{11}P_1$	O_1 PS 40:3	$[M+2Na-H]^+$	857.5782	0.27	False	NA	True	False	True	NA	False
11749	902.5487	298.57	$C_{46}H_{84}N_1O_{11}P_1$	O_3 PC 38:4	$[M+2Na-H]^+$	857.5782	0.27	False	NA	True	False	True	NA	False

PGs ($[M+NH_4]^+$), MGDGs ($[M+NH_4]^+$), and DGDGs ($[M+NH_4]^+$) are identical to the dominant adducts identified in the previous study using authentic standards or database information. Only annotations with dominant adducts were considered valid. If a pseudospectrum contained several different annotations as dominant adduct (e.g. O_1 PC 34:3 $[M+H]^+$, PC 36:5 $[M+H]^+$, and O_1 PC 36:4 $[M+H]^+$ in pseudospectrum 144; Table II) and one annotation occurred with additional adducts (O_1 PC 36:4 as $[M+Na]^+$), only this remained valid (Supplemental Table S1, Adduct filter = true). In addition to the removal of likely false-positive annotations, this filter step also reduces redundancy caused by identical annotations of different adducts formed by one analyte. In the aforementioned example, only the $[M+H]^+$ adduct of O_1 PC 36:4 passed this filter (Table II), providing strong support that pseudospectrum 144 is O_1 PC 36:4, represented most abundantly by the $[M+H]^+$ adduct, which also is the base peak of the pseudospectrum. This filter was found to be very effective. Its application resulted in a reduction of the number of annotations to 1,079.

Retention Filter

In untargeted metabolomics, retention time prediction can be used to validate mass-based compound annotations (Hagiwara et al., 2010; Cao et al., 2015). Lipids of the same class elute at similar retention times (Hummel et al., 2011). Lipids eluting much earlier or later than expected are most likely incorrectly annotated. To reduce their number, we followed a simplified approach that is independent of available compound polarity information or prediction models but is applicable to compound classes eluting in clusters, like the lipids studied in this work (Fig. 1, B–D). To remove annotations distant from the expected elution time point, we identified annotations (passing Isotope, Bothmode, and Adduct filters) within every lipid class that elute earlier or later than at maximum kernel density ± 3 sigma (false in Supplemental Table S1, Retention filter). Even though this procedure removed only a small number of putatively incorrect annotations in this already intensely filtered data set and none from the example pseudospectrum 144, this filter may be helpful in general to improve annotation reliability. Its application reduced the number of annotations to 1,066.

m/z Correction

Despite external and lock-mass calibration of every spectrum to minimize *m/z* errors, there was a linear deviation in the error distribution (Supplemental Fig. S1A). Small *m/z* values tend to have a negative error (the observed mass is lower than expected) and large *m/z* values tend to have a positive error more often, but the latter effect was less pronounced. Noteworthy, the average error was approximately zero around *m/z* 622.0289, the *m/z* of the compound used for lock-mass calibration. The *m/z* deviations depend on *m/z* value

and signal intensity in high-resolution MS, and solutions like linear or polynomial fitting were introduced to compensate for such drifts in order to improve mass accuracy (Mihaleva et al., 2008; Lommen et al., 2011). We followed the plausible argument of the authors to assume that we must have correctly annotated a certain number of lipid sum formulae because they are known to exist in our sample. We used the *m/z* of higher confidence lipid annotations (Isotope, Bothmode, Adduct, and Retention filters = true) as predictors in a linear model for the *m/z* error. The resulting model was used to fit and replace all *m/z* and related errors in the peaktable in five iterations (Supplemental Fig. S1, A–F). No correction greater than 0.6 mD was applied (Supplemental Fig. S1G). The resulting error distribution was tighter and more closely zero centered. We deduce an overall accuracy of below 1.5 ppm for all *m/z* features of the LC-MS analysis in positive mode (Supplemental Fig. S1D).

High-Throughput Posthoc Acquisition of MS/MS Spectra

In MS/MS experiments, lipids largely follow certain predictable fragmentation rules. Fragments and NLs can be assigned to acyl residues or head groups of specific glycerides, PL or GL. Thus, MS/MS fragmentation can be used to cross-validate oxylipid annotations based on accurate mass of the PR. Furthermore, the spectra reveal structural information on the molecular composition of the lipids and positional information of the oxidation. We followed a procedure similar to that described by Koelmel et al. (2017), but instead of using exclusion lists, we constructed a scheduled precursor list (SPL) from all potentially monoisotopic peaks from the profiling experiment. The benefit is that MS/MS spectra are collected more effectively, because no MS/MS spectra other than relevant are produced (i.e. from solvent contaminants, background signals, or isotopic peaks). We extracted retention time (±1 s) and *m/z* (±20 mD) of all potentially monoisotopic peaks from the profiling experiment to create the SPL (Supplemental Table S4) with 12,080 entries in a format applicable to the mass spectrometer. Aliquot extracts of the profiling experiment were rerun using identical HPLC settings but otherwise in auto-MS/MS mode. If an *m/z* of an MS (precursor) scan matched to a feature in the SPL, an MS/MS spectrum was recorded during the following scan. After each LC-MS/MS run, collected spectra were identified using retention time and *m/z* windows, and the corresponding entries were removed from the SPL. The next LC-MS/MS file was recorded with the reduced SPL. The cycle was stopped after 27 consecutive LC-MS/MS runs, because the remaining *m/z* in the SPL either did not trigger MS/MS scans or led to the recording of MS/MS spectra of very low intensity.

Following this procedure, we recorded 27 LC-MS/MS files with 9,937 nonredundant MS/MS spectra from a pooled sample. The whole procedure was repeated two more times. One repetition was made using extracts from two of the oldest ambient stored seed stocks from 1998, which were expected to be enriched in lipids formed during aging. This led to the recording of 9,941 MS/MS spectra. The other repetition was made using extracts from two younger seed stocks from 2002 (cold stored) and 2006 (ambient stored), which were expected to contain higher contents of lipids that would diminish during aging. This led to the recording of 10,419 MS/MS spectra. These repetitions gained additional and higher quality MS/MS spectra (detected as higher base peak abundance) for a large number of targets already fragmented from the pooled sample. A total of 8,957 nonredundant monoisotopic MS/MS spectra (Supplemental Fig. S2; Supplemental Table S1, MSMS mz, MSMS intensity, and MassIVE [ftp://massive.ucsd.edu/MSV000081200]) remained after processing and merging of the three data sets.

Automatized MS/MS Validation and Acyl Structure Annotation

The MS/MS fragmentation patterns of glycerides, PLs and GLs, have been analyzed extensively regarding acyl and head group composition (Byrdwell and Neff, 2002; Taguchi et al., 2005; Schwudke et al., 2006; Manicke et al., 2008; Ivanova et al., 2009; Murphy and Axelsen, 2011; Anesi and Guella, 2015; Bandu et al., 2016; Maciel et al., 2016), but the utilization of high-resolution MS/MS spectra for the identification and structural annotation of oxidized lipids was hitherto far less investigated (Vu et al., 2012). We found a high generalizability between nominal mass MS/MS spectra of authentic standards available at LIPID MAPS (www.lipidmaps.org) and the high-resolution MS/MS spectra for the corresponding lipids in our study (Supplemental Fig. S3). To be able to detect acyl and head groups of oxidized lipids, we extended the known fragmentation rules of nonoxidized lipids into rules expected for oxylipid fragmentation in high resolution (Supplemental Table S5).

Lipids containing a glycerol backbone and esterified FAs are expected to form four major types of fragments: FA ($[RCOOH+X]^+$ and $[RCO]^+$) and FA-glycerol fragments ($RCOOH+74+X]^+$ and $[RCO+74]^+$) and NLs of FAs ([RCOOX]), where R represents the alkyl residue of the FA and X represents the annotated adduct (H, Na, K, or NH_4). To identify oxylipid components, each FA structure also was allowed to have up to four additional oxygen atoms. This resulted in a total of 3,332 fragments and 1,375 NLs possible when acyl structures with 10 to 30 C atoms and zero to five double bonds were considered. The fragmentation library (Supplemental Table S5) also included fragments and NLs of head groups specific for the membrane lipid classes and NLs of adducts. The fragments/NLs of all 8,957 MS/MS spectra were annotated using this library with 5 mD tolerance, resulting in a file containing the annotations of 190,099 fragments/NLs (Supplemental Table S6). To reconstruct lipid compositions

from the annotated fragments, we generated a lipid structure library with all possible nonredundant FA-acyl combinations for lipids containing three FAs (TAGs), two FAs (DAGs, PCs, PEs, PGs, PIs, MGDG, and DGDG), and one FA (MAGs, lysoPCs, lysoPEs, lysoPGs, and lysoPIs). Allowing for 10 to 30 carbon and zero to five double bond(s) per FA and zero to four additional oxygen atom(s) per lipid (Supplemental Table S7), the list contained 1,729,805 lipids differing in FA/head group composition. In the following section, the applied structural annotation rules are explained in detail and on the basis of example MS/MS spectra for all the lipid classes in which oxidized lipids were detected.

TAGs were regarded as MS/MS validated (true in Supplemental Table S1, MSMS filter) if we were able to identify at least one NL and two additional NLs or fragments in the MS/MS spectrum, which combine to the TAG tentative sum formula. Only fragments/NLs with the predicted adduct of the parent ion or the protonated form of the fragments were allowed for the annotation.

MS/MS spectra were recorded for 276 out of the 302 TAG annotations that passed the filters described above (Table III). Two hundred fifty-four of these passed the MS/MS validation test (Table III; Supplemental Table S1, Source class = Triacylglycerol and All filters = true). Acyl compositions were determined for all of them, and their quantitative representation in the spectrum was determined as the sum of all explanatory fragments/NLs in percentage of the base peak of the MS/MS spectrum (Fig. 2; Supplemental Table S1, Putative composition). Table V lists all 254 TAGs and their highest ranking FA composition. For some of the 254 TAGs with MS/MS validation as $[M+NH_4]^+$ adduct, additional validation of sum formula and structural composition was gained from the MS/MS spectra of additional adducts. For example, O_1 TAG 50:2 in pseudospectrum 31 (Supplemental Table S1, pcgroup = 31) is reported as TAG (16:0/O_1 16:0/18:2) with highest fragment abundance in all three detected adducts ($[M+NH_4]^+$, $[M+H]^+$, and $[M+K]^+$), but only the $[M+NH_4]^+$ adduct remained among the valid (or, more precisely, nonredundant) annotations after the adduct filter step described above was carried out. The majority (167) of the 254 TAGs are oxidized (Tables IV and V). We annotated 87 nonoxidized TAGs: 82 O_1 TAGs, 44 O_2 TAGs, 23 O_3 TAGs, and 18 O_4 TAGs. The relative intensities also dropped with increasing oxidation levels (Table IV). The chromatographic pattern of all fully validated lipids plus FAs (for this class, it was not possible to apply generalizable MS/MS fragmentation patterns in this study) is displayed in Figure 1B. Figure 1, C and D, display the specific patterns for the intact and oxidized TAGs. The pattern for the intact TAGs (Fig. 1C) forms a mesh of signals in typical order: increasing retention times with increasing numbers of carbon atoms, decreasing retention times with increasing numbers of double bonds. Exactly the same pattern was reported in previous studies for TAGs (Giavalisco et al., 2011) and PCs (Hummel et al., 2011). The O_1 TAGs (Fig. 1C) form an almost identical mesh shifted highly reproducibly 40 to 50 s to an earlier elution time point. The same shift occurs with further elevations in oxidation level (Fig. 1D) but is blurred due to an increasing number of isomers among the oxidized lipids. We also saw this chromatographic shift of the oxidized lipids in all other classes discussed below (Supplemental Table S1).

While a large number of intact TAGs with certain abundances also are found in singly oxidized form, only the most abundant intact TAG species were found in higher oxidation states. With very few exceptions, O_2 TAGs were found only for TAGs with 50, 52, and 54 carbon atoms in the acyl chains, and $O_{3\text{-}4}$ TAGs were found only for 52 and 54 FA carbon TAGs. Figure 2A shows the MS/MS spectrum of the PR *m/z* 958.7342 (Supplemental Table S1, Formula_ID = 9409), putatively annotated as ammonium adduct of O_4 TAG 54:7 and passing all filters. One hundred thirty-two fragments/NLs were detected in the MS/MS spectrum (Supplemental Table S6, Mass_ID = 21399), and 99 of them are valid $[M+H]^+$/$[M+NH_4]^+$ fragments or

Table III. *Summary of MS/MS validation and acyl structure annotation of intact and oxidized lipids*

Lipid	Isotope, Bothmode, Adduct, and Retention Filtered Annotations	Isotope, Bothmode, Adduct, and Retention Filtered Annotations with Available MS/MS Spectrum	Isotope, Bothmode, Adduct, Retention, and MS/MS Filtered Annotations	Isotope, Bothmode, Adduct, Retention, and MS/MS Filtered Annotations with Structural Composition
O_0-O_4 TAG	302	276	254	254
O_0-O_4 DAG	154	148	121	121
O_0-O_4 MAG	34	29	10	10
O_0-O_4 PC	95	92	84	9
O_0-O_4 PE	66	59	19	11
O_0-O_4 PG	47	43	12	11
O_0-O_4 PI	10	9	7	5
O_0-O_4 lysoPC	31	28	25	25
O_0-O_4 lysoPE	18	15	11	11
O_0-O_4 lysoPG	5	3	2	2
O_0-O_4 lysoPI	2	2	0	0
O_0-O_4 MGDG	83	62	27	20
O_0-O_4 DGDG	65	62	52	37
All lipids	912	828	624	516

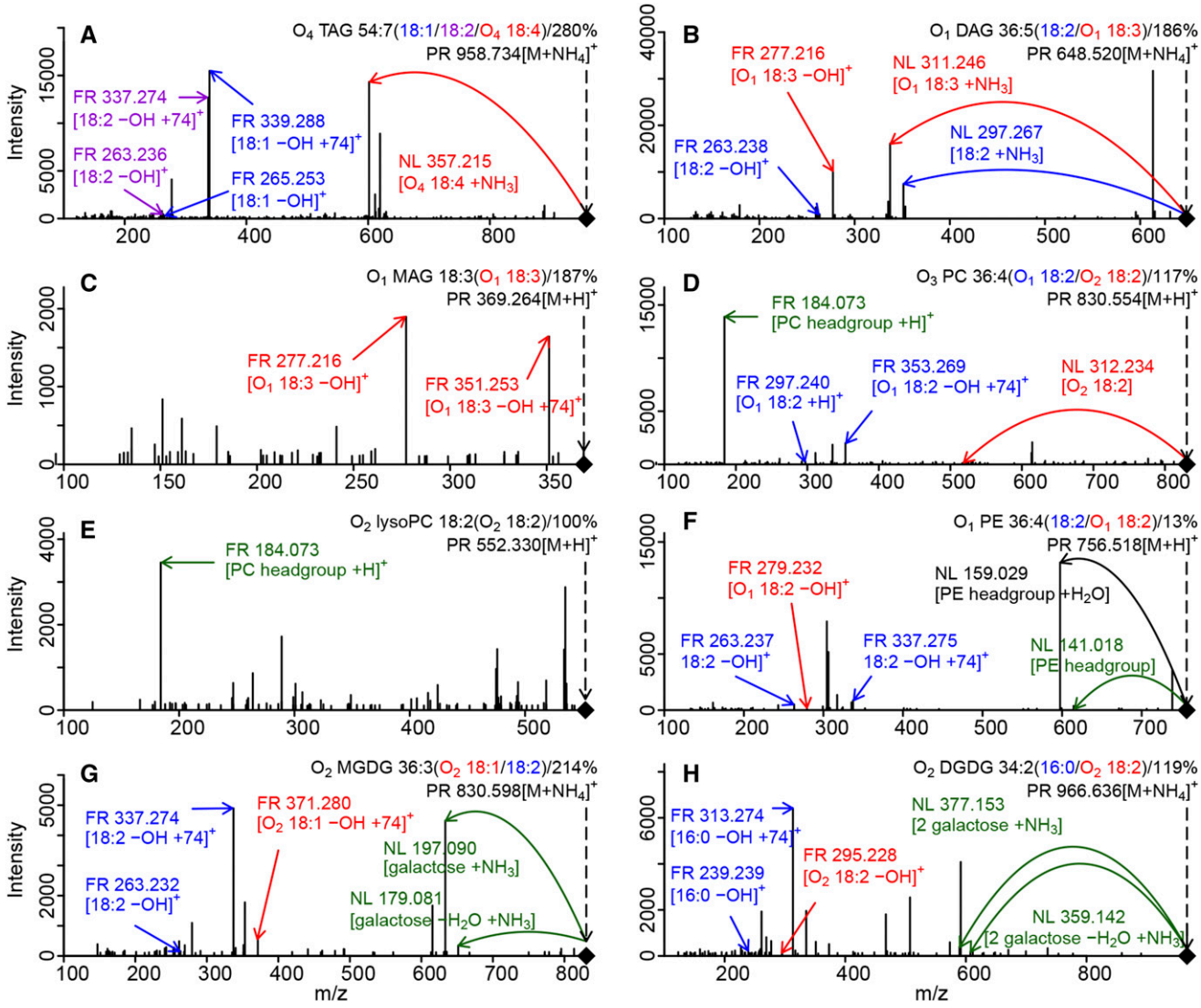

Figure 2. Examples of MS/MS validation and acyl composition determination for lipids of eight different classes. NLs and fragments (FR) of FAs and head groups were computationally identified and used to validate the PR annotation for O_4 TAG 54:7 (Supplemental Table S1, Formula_ID = 9409; for the chromatographic profile, see Fig. 1D [A]), O_1 DAG 36:5 (Formula_ID = 7380 [B]), O_1 MAG 18:3 (Formula_ID = 1302 [C]), O_3 PC 36:4 (Formula_ID = 2322 [D]), O_2 lysoPC 18:2 (Formula_ID = 1850 [E]), O_1 PE 36:4 (Formula_ID = 1440 [F]), O_2 MGDG 36:3 (Formula_ID = 8269 [G]), and O_2 DGDG 34:2 (Formula_ID = 8128 [H]). Only subsets of the indicated fragments are depicted. Multiple occurrences of the same FA within the different spectra are indicated by identical colors. FAs are labeled in purple, blue, or red, and head groups are labeled in green. Annotations in black were not obtained computationally and are only used to provide additional information in the example spectra. Representation of the acyl combination in the MS/MS spectra is expressed as cumulative abundance of all explanatory fragments/NLs in percentage of the base peak.

corresponding NLs. From 5,562 acyl combinations possible for O_4 TAG 54:7 (Supplemental Table S7, Name = O4 TAG 54:7), 86 combinations can be constructed (Supplemental Table S1, Putative composition) out of these 99 fragment/NLs annotations. The highest ranking acyl combination is 18:1/18:2/O_4 18:4, indicated by five fragments and one NL (Supplemental Table S6, Mass_ID = 21399 and Structure = 18:1 & 18:2 & O4-18:4). The sum of intensities of these five fragments (280%) relative to the base peak *m/z* 339.288 (100%) is the highest of all detected combinations. The FA O_4 18:4 was identified by an NL of the ammoniated FA (Δ*m/z* 357.2151) resulting in a fragment ion at *m/z* 601.5192. This fragment is characteristic for a protonated DAG 36:3 with a loss of one water molecule. For the remaining two nonoxidized FAs, four fragments were detected, indicating the loss of a hydroxyl group from the FA-glycerol fragments (*m/z* 339.2884 for FA 18:1 and *m/z* 337.2738 for FA 18:2) and the loss of a hydroxyl group from the FA fragments themselves (*m/z*

Table IV. *Number and relative content of identified intact and oxidized lipids*

Lipid	No. of Lipids						Relative Lipid Content				
	O_0–O_4	O_0	O_1	O_2	O_3	O_4	O_0	O_1	O_2	O_3	O_4
TAG	254	87	82	44	23	18	80.65	16.33	2.44	0.43	0.15
DAG	121	36	30	31	16	8	81.12	10.12	7.12	1.18	0.47
MAG	10	9	1	0	0	0	95.79	4.21	0	0	0
FA[a]	154	50	46	35	15	8	74.62	7.34	13.18	3.81	1.05
PC	84	33	16	23	8	4	94.14	3.95	1.56	0.29	0.07
PE	19	13	5	0	1	0	96.23	3.7	0	0.07	0
PG	12	12	0	0	0	0	100	0	0	0	0
PI	7	7	0	0	0	0	100	0	0	0	0
lysoPC	25	18	6	1	0	0	99.6	0.33	0.06	0	0
lysoPE	11	11	0	0	0	0	100	0	0	0	0
lysoPG	2	2	0	0	0	0	100	0	0	0	0
lysoPI	0	0	0	0	0	0	0	0	0	0	0
MGDG	27	10	9	7	1	0	89.33	9.08	1.48	0.11	0
DGDG	52	21	11	15	5	0	87.32	9.1	2.8	0.77	0
Sum/Mean	778	309	206	156	69	38	85.63	4.58	2.05	0.48	0.12

[a]Not MS/MS validated.

265.2529 for FA 18:1 and *m/z* 263.2355 for FA 18:2). We noticed that MS/MS spectra of nonoxidized TAGs typically display NLs indicative of all three FAs, whereas oxidized TAGs (and also DAGs) almost exclusively lose the oxidized FA and display fragments for the nonoxidized FAs. The highest ranking acyl combinations for all 254 identified TAGs are provided in Table V.

DAGs were regarded as validated if the NL of one FA coincided with the detection of a complementary FA as a fragment and that in combination form the expected sum formula of the DAG. MS/MS spectra were available for 148 out of 154 annotations left after retention filtering. One hundred twenty-one of these were MS/MS validated and structurally annotated (Table III; Supplemental Table S1). For example, four acyl combinations were detected for a precursor *m/z* 648.5199 (Supplemental Table S1, Formula_ID = 7380), annotated as ammonium adduct of O_1 DAG 36:5. Of these structures, the combination O_1 18:3/18:2 exerted the highest spectral abundance (186%) and was supported by seven MS/MS fragments (Supplemental Table S6). The ammoniated O_1 DAG 36:5 produces characteristic, although unspecific, fragments (Fig. 2B) by NL of NH_3 ($\Delta m/z$ 17.0263), NH_3 and H_2O ($\Delta m/z$ 35.0366), but also specific ammoniated FA fragments ($\Delta m/z$ 311.2455 for FA O_1 18:3 and $\Delta m/z$ 297.2666 for FA 18:2). Each NL of an FA results in a fragment of the remaining FA-glycerol fragment with a loss of a hydroxyl group (*m/z* 337.2743 for FA 18:2 and *m/z* 351.2532 for FA O_1 18:3), but these annotations are redundant to the NL annotation and, thus, were not considered in the validation procedure. Three independent fragments could be assigned to this FA combination. The fragments *m/z* 277.2160 and 263.2375 were generated by a loss of H_2O of the protonated FA O_1 18:3 and 18:2, whereas *m/z* 295.2280 (not labeled in Fig. 2B) indicates the protonated FA O_1 18:3. Thus, O_1 DAG 36:5 and its most representative structure (18:2/O_1 18:3) is actually MS/MS validated by two observation combinations: NL of FA 18:2 coinciding with a fragment of FA O_1 18:3 and NL of FA O_1 18:3 coinciding with a fragment of FA 18:2.

MAGs were regarded as validated if the expected FA was detected as a result of a glycerol NL. Sixteen annotations were validated by all filters (Table III). For example, O_1 MAG 18:3 (Supplemental Table S1, Formula_ID = 1302) was MS/MS validated by detection of the fragment for the FA O_1 18:3 (*m/z* 277.2167) resulting from an NL of ammonia, water, and glycerol (Fig. 2C). The base peak *m/z* 351.2537 corresponds to an FA-glycerol fragment with a loss of a hydroxyl group resulting from an NL of NH_3 and H_2O ($\Delta m/z$ 35.0366), but we judged this constellation too unspecific for validation, even though the precursor was annotated as ammonium adduct.

PLs were regarded as MS/MS validated when we detected a fragment or NL specific for the corresponding head group (Bandu et al., 2016) in combination with the predicted adduct or in protonated form. We scanned for intact and oxidized PC, PE, PG, PI, and their lysoforms, but only for PC, lysoPC, and PE were oxidized lipids MS/MS validated (Table IV). Acyl combinations were identified if FA fragments/NLs in any combination match the predicted sum formula. In the majority of cases, it was not possible to determine the acyl composition of PLs, because their MS/MS spectra often were dominated by the head group. For only 36 out of the 122 fully validated structures, we could reconstruct the FA composition. Remarkably, and in strong contrast to the situation found for the DAGs, there was in almost all cases only one putative composition detected for the 36 PCs, PEs, PGs, and PIs. Lysophospholipids were structurally annotated already when they were MS/MS validated by identification of the head group, because they possess only one FA.

PCs were MS/MS validated if the PC head group ($C_5H_{14}NO_4P$) was detected as a fragment or NL in combination with the expected adduct or protonated.

Table V. *TAG acyl compositions*

The acyl composition of example Formula_ID 9409 is shown in boldface. For chromatographic distribution in the LC-MS analysis, see Figure 1D, and for MS/MS spectra, see Figure 2A. Rt, Retention time (in seconds).

Formula_ID	*m/z*	Rt	Formula	Name	Acyl Composition[a]	Formula_ID	*m/z*	Rt	Formula	Name	Acyl Composition[a]
7800	776.6402	445.0	$C_{47}H_{82}O_7$	O_1 44:4	16:0/18:2/O_1 10:2; 211%	8498	902.7439	457.2	$C_{55}H_{96}O_8$	O_2 52:5	16:0/O_1 18:2/O_1 18:3; 227%
7801	778.6546	461.5	$C_{47}H_{84}O_7$	O_1 44:3	16:0/16:0/O_1 12:3; 68%	8496	902.7440	464.3	$C_{55}H_{96}O_8$	O_2 52:5	16:0/O_1 18:2/O_1 18:3; 346%
7185	786.6604	492.6	$C_{49}H_{84}O_6$	46:5	10:1/18:2/18:2; 55%	8499	902.7445	486.0	$C_{55}H_{96}O_8$	O_2 52:5	16:0/18:2/O_2 18:3; 179%
7186	788.6763	504.2	$C_{49}H_{86}O_6$	46:4	10:0/18:2/18:2; 130%	8500	902.7445	478.4	$C_{55}H_{96}O_8$	O_2 52:5	16:0/18:2/O_2 18:3; 301%
7187	788.6764	511.8	$C_{49}H_{86}O_6$	46:4	10:0/18:2/18:2; 71%	7225	902.8168	598.6	$C_{57}H_{104}O_6$	54:3	18:0/18:1/18:2; 132%
7188	790.6917	522.4	$C_{49}H_{88}O_6$	46:3	10:0/18:1/18:2; 249%	8503	904.7592	458.7	$C_{55}H_{98}O_8$	O_2 52:4	16:0/18:3/O_2 18:1; 169%
7189	792.7076	539.6	$C_{49}H_{90}O_6$	46:2	12:0/16:0/18:2; 294%	8502	904.7594	476.9	$C_{55}H_{98}O_8$	O_2 52:4	16:0/O_1 18:2/O_1 18:2; 179%
7803	804.6711	459.7	$C_{49}H_{86}O_7$	O_1 46:4	16:0/18:2/O_1 12:2; 212%	8504	904.7604	496.1	$C_{55}H_{98}O_8$	O_2 52:4	16:0/18:2/O_2 18:2; 146%
7804	806.6863	475.9	$C_{49}H_{88}O_7$	O_1 46:3	16:0/16:0/O_1 14:3; 127%	7227	904.8325	614.3	$C_{57}H_{106}O_6$	54:2	18:0/18:1/18:1; 173%
7190	816.7074	523.9	$C_{51}H_{90}O_6$	48:4	12:0/18:2/18:2; 168%	7860	906.7180	459.8	$C_{57}H_{92}O_7$	O_1 54:9	18:2/18:3/O_1 18:4; 259%
7191	816.7075	533.0	$C_{51}H_{90}O_6$	48:4	14:2/16:0/18:2; 249%	7861	906.7184	499.6	$C_{57}H_{92}O_7$	O_1 54:9	18:2/18:4/O_1 18:3; 115%
7192	818.7230	550.7	$C_{51}H_{92}O_6$	48:3	14:1/16:0/18:2; 219%	8486	906.7747	484.0	$C_{55}H_{100}O_8$	O_2 52:3	16:0/18:2/O_2 18:1; 179%
7193	818.7230	542.1	$C_{51}H_{92}O_6$	48:3	14:1/16:0/18:2; 261%	8487	906.7760	508.2	$C_{55}H_{100}O_8$	O_2 52:3	16:0/18:2/O_2 18:1; 134%
8473	820.6662	438.5	$C_{49}H_{86}O_8$	O_2 46:4	16:0/18:2/O_2 12:2; 21%	7228	906.8480	629.9	$C_{57}H_{108}O_6$	54:1	16:0/18:1/20:0; 297%
7194	820.7386	559.3	$C_{51}H_{94}O_6$	48:2	14:0/16:0/18:2; 307%	7863	908.7327	459.2	$C_{57}H_{94}O_7$	O_1 54:8	18:3/18:4/O_1 18:1; 81%
7195	820.7389	569.9	$C_{51}H_{94}O_6$	48:2	14:0/16:0/18:2; 294%	7862	908.7334	474.9	$C_{57}H_{94}O_7$	O_1 54:8	18:2/18:3/O_1 18:3; 283%
7196	822.7545	576.9	$C_{51}H_{96}O_6$	48:1	14:0/16:0/18:1; 177%	8489	908.7902	501.2	$C_{55}H_{102}O_8$	O_2 52:2	16:0/18:1/O_2 18:1; 157%
7197	824.7700	594.6	$C_{51}H_{98}O_6$	48:0	16:0/16:0/16:0; 105%	7229	908.8638	646.1	$C_{57}H_{110}O_6$	54:0	16:0/16:0/22:0; 165%
7807	830.6877	461.2	$C_{51}H_{88}O_7$	O_1 48:5	16:0/18:2/O_1 14:3; 33%	7865	910.7480	470.8	$C_{57}H_{96}O_7$	O_1 54:7	18:2/18:4/O_1 18:1; 95%
7809	834.7178	488.5	$C_{51}H_{92}O_7$	O_1 48:3	16:0/16:2/O_1 16:1; 32%	7864	910.7491	489.5	$C_{57}H_{96}O_7$	O_1 54:7	18:2/18:2/O_1 18:3; 205%
7810	834.7182	500.6	$C_{51}H_{92}O_7$	O_1 48:3	14:0/16:0/O_1 18:3; 259%	7866	912.7638	486.5	$C_{57}H_{98}O_7$	O_1 54:6	18:2/18:3/O_1 18:1; 76%
7811	836.7330	493.3	$C_{51}H_{94}O_7$	O_1 48:2	14:0/18:2/O_1 16:0; 112%	7867	912.7648	504.7	$C_{57}H_{98}O_7$	O_1 54:6	18:2/18:2/O_1 18:2; 196%
7812	836.7342	514.3	$C_{51}H_{94}O_7$	O_1 48:2	14:0/16:0/O_1 18:2; 286%	7854	914.7803	522.4	$C_{57}H_{100}O_7$	O_1 54:5	18:1/18:2/O_1 18:2; 271%
7201	838.6924	499.1	$C_{53}H_{88}O_6$	50:7	14:3/18:1/18:3; 74%	8961	916.7229	408.2	$C_{55}H_{94}O_9$	O_3 52:6	16:0/O_1 18:4/O_2 18:2; 145%
7814	838.7499	529.8	$C_{51}H_{96}O_7$	O_1 48:1	16:0/16:0/O_1 16:1; 169%	8962	916.7238	424.8	$C_{55}H_{94}O_9$	O_3 52:6	16:0/O_1 18:3/O_2 18:3; 298%
7202	840.7074	514.8	$C_{53}H_{90}O_6$	50:6	14:2/18:2/18:2; 181%	7855	916.7959	540.2	$C_{57}H_{102}O_7$	O_1 54:4	18:1/18:1/O_1 18:2; 225%
7815	840.7643	529.5	$C_{51}H_{98}O_7$	O_1 48:0	16:0/16:0/O_1 16:0; 116%	7856	916.7959	553.2	$C_{57}H_{102}O_7$	O_1 54:4	16:1/18:1/O_1 20:2; 61%
7203	842.7229	525.9	$C_{53}H_{92}O_6$	50:5	14:0/18:2/18:3; 297%	8964	918.7378	407.7	$C_{55}H_{96}O_9$	O_3 52:5	16:0/O_1 18:4/O_2 18:1; 81%
7204	842.7231	533.5	$C_{53}H_{92}O_6$	50:5	14:1/18:2/18:2; 193%	8963	918.7384	423.3	$C_{55}H_{96}O_9$	O_3 52:5	16:0/O_1 18:3/O_2 18:2; 76%
7205	844.7386	543.1	$C_{53}H_{94}O_6$	50:4	14:0/18:2/18:2; 172%	8965	918.7389	441.0	$C_{55}H_{96}O_9$	O_3 52:5	16:0/O_1 18:3/O_2 18:2; 226%
7207	846.7541	588.5	$C_{53}H_{96}O_6$	50:3	16:0/16:1/18:2; 112%	7857	918.8116	556.8	$C_{57}H_{104}O_7$	O_1 54:3	16:0/18:2/O_1 20:1; 52%
7206	846.7544	560.8	$C_{53}H_{96}O_6$	50:3	16:0/16:0/18:3; 163%	8967	920.7544	440.5	$C_{55}H_{98}O_9$	O_3 52:4	16:0/18:3/O_3 18:1; 174%
7209	848.7700	603.2	$C_{53}H_{98}O_6$	50:2	16:0/16:1/18:1; 114%	7249	920.7692	532.5	$C_{59}H_{98}O_6$	56:8	18:2/18:3/20:3; 98%
7208	848.7704	577.9	$C_{53}H_{98}O_6$	50:2	16:0/16:0/18:2; 149%	7858	920.8268	574.4	$C_{57}H_{106}O_7$	O_1 54:2	16:0/18:1/O_1 20:1; 57%
7198	850.7856	595.6	$C_{53}H_{100}O_6$	50:1	16:0/16:0/18:1; 145%	8515	922.7131	410.2	$C_{57}H_{92}O_8$	O_2 54:9	18:4/O_1 18:2/O_1 18:3; 161%
7199	852.8010	612.3	$C_{53}H_{102}O_6$	50:0	16:0/16:0/18:0; 166%	8513	922.7132	423.4	$C_{57}H_{92}O_8$	O_2 54:9	18:4/O_1 18:2/O_1 18:3; 229%
7820	854.6866	446.6	$C_{53}H_{88}O_7$	O_1 50:7	18:2/18:2/O_1 14:3; 43%	8514	922.7134	442.0	$C_{57}H_{92}O_8$	O_2 54:9	18:4/O_1 18:2/O_1 18:3; 139%
7821	856.7024	465.1	$C_{53}H_{90}O_7$	O_1 50:6	18:1/18:2/O_1 14:3; 4%	8959	922.7698	445.9	$C_{55}H_{100}O_9$	O_3 52:3	16:0/18:2/O_3 18:1; 128%
7823	858.7177	472.3	$C_{53}H_{92}O_7$	O_1 50:5	18:2/18:3/O_1 14:0; 20%	7239	922.7852	550.2	$C_{59}H_{100}O_6$	56:7	18:2/18:3/20:2; 226%
7824	858.7185	484.0	$C_{53}H_{92}O_7$	O_1 50:5	14:0/18:2/O_1 18:3; 20%	7859	922.8431	602.7	$C_{57}H_{108}O_7$	O_1 54:1	16:0/18:1/O_1 20:0; 64%
7826	860.7338	499.1	$C_{53}H_{94}O_7$	O_1 50:4	14:0/18:2/O_1 18:2; 237%	8518	924.7273	408.7	$C_{57}H_{94}O_8$	O_2 54:8	18:4/18:4/O_2 18:0; 36%
7827	862.7484	503.2	$C_{53}H_{96}O_7$	O_1 50:3	16:0/18:3/O_1 16:0; 85%	8516	924.7279	422.1	$C_{57}H_{94}O_8$	O_2 54:8	18:4/O_1 18:1/O_1 18:3; 171%
7829	862.7487	496.1	$C_{53}H_{96}O_7$	O_1 50:3	16:0/18:3/O_1 16:0; 140%	8517	924.7282	437.0	$C_{57}H_{94}O_8$	O_2 54:8	18:4/O_1 18:1/O_1 18:3; 219%
7828	862.7492	513.8	$C_{53}H_{96}O_7$	O_1 50:3	16:0/18:2/O_1 16:1; 235%	8519	924.7286	456.2	$C_{57}H_{94}O_8$	O_2 54:8	18:2/O_1 18:2/O_1 18:4; 210%

(*Table continues on following page.*)

Table V. (*Continued from previous page.*)

Formula_ID	*m/z*	Rt	Formula	Name	Acyl Composition[a]	Formula_ID	*m/z*	Rt	Formula	Name	Acyl Composition[a]
7830	862.7493	521.9	$C_{53}H_{96}O_7$	O_1 50:3	16:0/16:0/O_1 18:3; 190%	8960	924.7849	461.7	$C_{55}H_{102}O_9$	O_3 52:2	16:0/18:1/O_3 18:1; 7%
7833	864.7644	513.3	$C_{53}H_{98}O_7$	O_1 50:2	16:0/18:2/O_1 16:0; 125%	7240	924.8007	567.0	$C_{59}H_{102}O_6$	56:6	18:2/18:3/20:1; 272%
7834	864.7647	552.3	$C_{53}H_{98}O_7$	O_1 50:2	16:0/18:2/O_1 16:0; 12%	8521	926.7435	433.9	$C_{57}H_{96}O_8$	O_2 54:7	18:4/O_1 18:1/O_1 18:2; 235%
7832	864.7648	534.5	$C_{53}H_{98}O_7$	O_1 50:2	16:0/16:0/O_1 18:2; 179%	8522	926.7438	450.6	$C_{57}H_{96}O_8$	O_2 54:7	18:2/O_1 18:2/O_1 18:3; 314%
7214	866.7236	511.8	$C_{55}H_{92}O_6$	52:7	16:0/18:2/18:5; 98%	8523	926.7444	464.8	$C_{57}H_{96}O_8$	O_2 54:7	18:2/18:3/O_2 18:2; 260%
7817	866.7798	550.2	$C_{53}H_{100}O_7$	O_1 50:1	16:0/16:0/O_1 18:1; 188%	7242	926.8165	583.5	$C_{59}H_{104}O_6$	56:5	18:2/18:2/20:1; 189%
7215	868.7386	528.4	$C_{55}H_{94}O_6$	52:6	16:0/18:3/18:3; 184%	7243	926.8170	603.2	$C_{59}H_{104}O_6$	56:5	18:1/18:2/20:2; 25%
7217	870.7541	572.9	$C_{55}H_{96}O_6$	52:5	16:1/18:1/18:3; 167%	8526	928.7589	446.6	$C_{57}H_{98}O_8$	O_2 54:6	18:3/O_1 18:1/O_1 18:2; 270%
7216	870.7545	545.1	$C_{55}H_{96}O_6$	52:5	16:0/18:2/18:3; 345%	8527	928.7592	463.2	$C_{57}H_{98}O_8$	O_2 54:6	18:3/O_1 18:1/O_1 18:2; 205%
7218	872.7698	587.5	$C_{55}H_{98}O_6$	52:4	16:1/18:1/18:2; 214%	7244	928.8323	599.6	$C_{59}H_{106}O_6$	56:4	18:1/18:2/20:1; 254%
7220	872.7699	603.7	$C_{55}H_{98}O_6$	52:4	16:0/18:2/18:2; 173%	8506	930.7744	468.3	$C_{57}H_{100}O_8$	O_2 54:5	18:2/O_1 18:1/O_1 18:2; 193%
7219	872.7710	562.8	$C_{55}H_{98}O_6$	52:4	16:0/18:2/18:2; 186%	7245	930.8480	615.3	$C_{59}H_{108}O_6$	56:3	18:1/18:2/20:0; 197%
7210	874.7860	580.5	$C_{55}H_{100}O_6$	52:3	16:0/18:1/18:2; 306%	9394	932.7183	410.2	$C_{55}H_{94}O_{10}$	O_4 52:6	16:0/O_2 18:3/O_2 18:3; 306%
8477	876.7278	458.2	$C_{53}H_{94}O_8$	O_2 50:4	16:0/O_1 16:1/O_1 18:3; 107%	8508	932.7898	485.5	$C_{57}H_{102}O_8$	O_2 54:4	18:1/18:2/O_2 18:1; 197%
7211	876.8013	597.1	$C_{55}H_{102}O_6$	52:2	16:0/18:1/18:1; 165%	7246	932.8636	631.0	$C_{59}H_{110}O_6$	56:2	16:0/18:1/22:1; 182%
8480	878.7436	457.2	$C_{53}H_{96}O_8$	O_2 50:3	16:0/O_1 16:0/O_1 18:3; 182%	9395	934.7328	421.3	$C_{55}H_{96}O_{10}$	O_4 52:5	16:0/O_1 18:3/O_3 18:2; 95%
8479	878.7441	470.8	$C_{53}H_{96}O_8$	O_2 50:3	16:0/O_1 16:1/O_1 18:2; 342%	9396	934.7335	409.2	$C_{55}H_{96}O_{10}$	O_4 52:5	16:0/O_1 18:4/O_3 18:1; 68%
7212	878.8167	613.3	$C_{55}H_{104}O_6$	52:1	16:0/18:0/18:1; 288%	8510	934.8060	503.2	$C_{57}H_{104}O_8$	O_2 54:3	16:0/18:2/O_2 20:1; 39%
8481	880.7594	469.9	$C_{53}H_{98}O_8$	O_2 50:2	16:0/O_1 16:0/O_1 18:2; 158%	7247	934.8792	646.1	$C_{59}H_{112}O_6$	56:1	16:0/18:1/22:0; 289%
8484	880.7596	494.5	$C_{53}H_{98}O_8$	O_2 50:2	16:0/16:0/O_2 18:2; 124%	9397	936.7488	420.3	$C_{55}H_{98}O_{10}$	O_4 52:4	16:0/O_1 18:3/O_3 18:1; 248%
8483	880.7597	485.5	$C_{53}H_{98}O_8$	O_2 50:2	16:0/16:0/O_2 18:2; 69%	9398	936.7491	436.5	$C_{55}H_{98}O_{10}$	O_4 52:4	16:0/18:2/O_4 18:2; 55%
8482	880.7599	509.7	$C_{53}H_{98}O_8$	O_2 50:2	16:0/16:0/O_2 18:2; 105%	7879	936.7647	493.6	$C_{59}H_{98}O_7$	O_1 56:8	16:1/18:2/O_1 22:5; 29%
7213	880.8319	629.4	$C_{55}H_{106}O_6$	52:0	16:0/18:0/18:0; 208%	8511	936.8208	521.9	$C_{57}H_{106}O_8$	O_2 54:2	16:0/18:2/O_2 20:0; 12%
7842	882.7180	473.4	$C_{55}H_{92}O_7$	O_1 52:7	16:0/18:3/O_1 18:4; 284%	7248	936.8949	663.2	$C_{59}H_{114}O_6$	56:0	16:0/16:0/24:0; 152%
8475	882.7756	499.6	$C_{53}H_{100}O_8$	O_2 50:1	16:0/16:0/O_2 18:1; 126%	8978	938.7073	392.2	$C_{57}H_{92}O_9$	O_3 54:9	18:4/O_1 18:3/O_2 18:2; 303%
7844	884.7330	464.8	$C_{55}H_{94}O_7$	O_1 52:6	16:1/18:3/O_1 18:2; 110%	8977	938.7075	407.7	$C_{57}H_{92}O_9$	O_3 54:9	O_1 18:2/O_1 18:3/O_1 18:4; 134%
7845	884.7331	473.4	$C_{55}H_{94}O_7$	O_1 52:6	16:0/18:3/O_1 18:3; 42%	7868	938.7805	510.7	$C_{59}H_{100}O_7$	O_1 56:7	18:2/18:3/O_1 20:2; 71%
7843	884.7334	489.5	$C_{55}H_{94}O_7$	O_1 52:6	16:0/18:3/O_1 18:3; 318%	8979	940.7226	407.4	$C_{57}H_{94}O_9$	O_3 54:8	18:3/O_1 18:2/O_2 18:3; 243%
7846	884.7335	481.9	$C_{55}H_{94}O_7$	O_1 52:6	18:2/18:3/O_1 16:1; 293%	8981	940.7227	384.9	$C_{57}H_{94}O_9$	O_3 54:8	18:4/O_1 18:2/O_2 18:2; 31%
7849	886.7485	481.5	$C_{55}H_{96}O_7$	O_1 52:5	18:2/18:3/O_1 16:0; 127%	8980	940.7232	419.8	$C_{57}H_{94}O_9$	O_3 54:8	18:4/O_1 18:1/O_2 18:3; 316%
7848	886.7492	505.2	$C_{55}H_{96}O_7$	O_1 52:5	16:0/18:2/O_1 18:3; 335%	9392	940.7794	410.2	$C_{55}H_{102}O_{10}$	O_4 52:2	16:0/O_1 18:2/O_3 18:0; 211%
7850	886.7502	535.5	$C_{55}H_{96}O_7$	O_1 52:5	16:0/18:2/O_1 18:3; 80%	7869	940.7947	505.7	$C_{59}H_{102}O_7$	O_1 56:6	18:2/18:4/O_1 20:0; 73%
7851	888.7642	498.6	$C_{55}H_{98}O_7$	O_1 52:4	16:0/18:3/O_1 18:1; 81%	7870	940.7960	527.4	$C_{59}H_{102}O_7$	O_1 56:6	18:2/18:3/O_1 20:1; 38%
7852	888.7648	519.9	$C_{55}H_{98}O_7$	O_1 52:4	16:0/18:2/O_1 18:2; 280%	8982	942.7381	384.0	$C_{57}H_{96}O_9$	O_3 54:7	18:3/O_1 18:3/O_2 18:1; 73%
7230	890.7236	497.1	$C_{57}H_{92}O_6$	54:9	18:1/18:3/18:5; 81%	8985	942.7381	399.1	$C_{57}H_{96}O_9$	O_3 54:7	18:4/O_1 18:2/O_2 18:1; 124%
7836	890.7796	515.3	$C_{55}H_{100}O_7$	O_1 52:3	18:1/18:2/O_1 16:0; 131%	8983	942.7383	408.3	$C_{57}H_{96}O_9$	O_3 54:7	18:4/O_1 18:1/O_2 18:2; 288%
7835	890.7803	537.6	$C_{55}H_{100}O_7$	O_1 52:3	16:0/18:1/O_1 18:2; 290%	8984	942.7385	418.3	$C_{57}H_{96}O_9$	O_3 54:7	18:2/O_1 18:3/O_2 18:2; 232%
7231	892.7385	513.8	$C_{57}H_{94}O_6$	54:8	18:2/18:3/18:3; 192%	8986	942.7394	428.9	$C_{57}H_{96}O_9$	O_3 54:7	18:4/O_1 18:1/O_2 18:2; 225%
7838	892.7958	554.2	$C_{55}H_{102}O_7$	O_1 52:2	16:0/18:0/O_1 18:2; 278%	7872	942.8116	541.6	$C_{59}H_{104}O_7$	O_1 56:5	18:2/18:2/O_1 20:1; 62%
7233	894.7542	554.2	$C_{57}H_{96}O_6$	54:7	18:2/18:2/18:3; 124%	8990	944.7541	427.4	$C_{57}H_{98}O_9$	O_3 54:6	18:3/O_1 18:2/O_2 18:1; 260%
7232	894.7544	530.5	$C_{57}H_{96}O_6$	54:7	18:2/18:2/18:3; 179%	7873	944.8272	559.3	$C_{59}H_{106}O_7$	O_1 56:4	18:1/18:2/O_1 20:1; 92%
7235	896.7698	570.4	$C_{57}H_{98}O_6$	54:6	18:1/18:2/18:3; 185%	8972	946.7703	434.2	$C_{57}H_{100}O_9$	O_3 54:5	12:3/O_1 18:1/O_2 24:1; 141%
7237	896.7700	590.0	$C_{57}H_{98}O_6$	54:6	18:2/18:2/18:2; 3%	8973	946.7711	443.0	$C_{57}H_{100}O_9$	O_3 54:5	18:1/18:2/O_3 18:2; 154%
7236	896.7708	548.2	$C_{57}H_{98}O_6$	54:6	18:1/18:2/18:3; 140%	7874	946.8425	574.9	$C_{59}H_{108}O_7$	O_1 56:3	16:0/22:1/O_1 18:2; 60%
8491	898.7123	432.2	$C_{55}H_{92}O_8$	O_2 52:7	18:4/O_1 16:0/O_1 18:3; 50%	7876	948.8585	593.1	$C_{59}H_{110}O_7$	O_1 56:2	16:0/20:1/O_1 20:1; 41%
8955	898.7708	458.7	$C_{53}H_{100}O_9$	O_3 50:1	16:0/16:0/O_3 18:1; 83%	7255	952.8322	585.0	$C_{61}H_{106}O_6$	58:6	18:2/18:3/22:1; 265%

(*Table continues on following page.*)

Table V. (*Continued from previous page.*)

Formula_ID	*m/z*	Rt	Formula	Name	Acyl Composition[a]	Formula_ID	*m/z*	Rt	Formula	Name	Acyl Composition[a]
7222	898.7851	587.5	$C_{57}H_{100}O_6$	54:5	18:0/18:2/18:3; 177%	7877	952.8898	625.4	$C_{59}H_{114}O_7$	O_1 56:0	18:0/18:0/O_1 20:0; 102%
7221	898.7858	565.8	$C_{57}H_{100}O_6$	54:5	18:1/18:2/18:2; 185%	7256	954.8479	600.6	$C_{61}H_{108}O_6$	58:5	18:2/18:2/22:1; 194%
8493	900.7278	429.4	$C_{55}H_{94}O_8$	O_2 52:6	18:4/O_1 16:0/O_1 18:2; 203%	9408	956.7176	364.2	$C_{57}H_{94}O_{10}$	O_4 54:8	18:2/18:2/O_4 18:4; 153%
8492	900.7280	448.6	$C_{55}H_{94}O_8$	O_2 52:6	16:0/O_1 18:3/O_1 18:3; 215%	9407	956.7178	372.3	$C_{57}H_{94}O_{10}$	O_4 54:8	18:2/18:2/O_4 18:4; 131%
7224	900.8006	603.2	$C_{57}H_{102}O_6$	54:4	18:1/18:1/18:2; 126%	9406	956.7180	383.6	$C_{57}H_{94}O_{10}$	O_4 54:8	18:4/O_2 18:2/O_2 18:2; 167%
7223	900.8012	582.5	$C_{57}H_{102}O_6$	54:4	18:1/18:1/18:2; 187%	**9409**	**958.7341**	**382.9**	**$C_{57}H_{96}O_{10}$**	**O_4 54:7**	**18:1/18:2/O_4 18:4; 280%**
8497	902.7429	432.9	$C_{55}H_{96}O_8$	O_2 52:5	16:0/O_1 18:1/O_1 18:4; 48%	9410	958.7351	397.1	$C_{57}H_{96}O_{10}$	O_4 54:7	18:2/O_1 18:3/O_3 18:2; 270%
8495	902.7436	445.1	$C_{55}H_{96}O_8$	O_2 52:5	16:0/O_1 18:2/O_1 18:3; 137%	8531	958.8051	481.9	$C_{59}H_{104}O_8$	O_2 56:5	18:2/18:3/O_2 20:0; 51%
7258	958.8793	631.4	$C_{61}H_{112}O_6$	58:3	18:1/18:2/22:0; 309%	7902	996.8583	567.9	$C_{63}H_{110}O_7$	O_1 60:6	18:2/24:1/O_1 18:3; 229%
9412	960.7486	358.7	$C_{57}H_{98}O_{10}$	O_4 54:6	18:2/18:3/O_4 18:1; 173%	7905	998.8737	578.9	$C_{63}H_{112}O_7$	O_1 60:5	18:2/24:1/O_1 18:2; 290%
9411	960.7493	380.4	$C_{57}H_{98}O_{10}$	O_4 54:6	18:1/18:2/O_4 18:3; 286%	7906	998.8738	586.0	$C_{63}H_{112}O_7$	O_1 60:5	18:2/24:0/O_1 18:3; 353%
9415	960.7499	393.7	$C_{57}H_{98}O_{10}$	O_4 54:6	18:1/18:2/O_4 18:3; 283%	7908	1000.8895	598.1	$C_{63}H_{114}O_7$	O_1 60:4	18:2/24:0/O_1 18:2; 255%
9413	960.7501	408.1	$C_{57}H_{98}O_{10}$	O_4 54:6	18:2/O_1 18:3/O_3 18:1; 291%	7909	1002.9049	613.8	$C_{63}H_{116}O_7$	O_1 60:3	18:1/18:2/O_1 24:0; 16%
9414	960.7505	423.9	$C_{57}H_{98}O_{10}$	O_4 54:6	18:2/18:3/O_4 18:1; 235%	7911	1004.9208	628.4	$C_{63}H_{118}O_7$	O_1 60:2	16:0/24:1/O_1 20:1; 36%
7259	960.8949	647.6	$C_{61}H_{114}O_6$	58:2	16:0/18:2/24:0; 312%	7272	1008.8945	618.8	$C_{65}H_{114}O_6$	62:6	18:2/18:3/26:1; 337%
9400	962.7637	396.0	$C_{57}H_{100}O_{10}$	O_4 54:5	18:1/18:1/O_4 18:3; 151%	7912	1008.9511	657.5	$C_{63}H_{122}O_7$	O_1 60:0	18:0/22:0/O_1 20:0; 189%
7260	962.9108	663.2	$C_{61}H_{116}O_6$	58:1	16:0/18:1/24:0; 304%	7273	1010.9109	634.5	$C_{65}H_{116}O_6$	62:5	18:2/18:3/26:0; 226%
7261	964.9263	681.4	$C_{61}H_{118}O_6$	58:0	16:0/16:0/26:0; 158%	7274	1012.9261	650.1	$C_{65}H_{118}O_6$	62:4	18:2/18:2/26:0; 190%
7884	966.8106	530.5	$C_{61}H_{104}O_7$	O_1 58:7	18:3/22:1/O_1 18:3; 41%	7275	1014.9421	665.2	$C_{65}H_{120}O_6$	62:3	18:1/18:2/26:0; 243%
7886	968.8273	544.1	$C_{61}H_{106}O_7$	O_1 58:6	18:2/22:1/O_1 18:3; 296%	7276	1016.9573	682.3	$C_{65}H_{122}O_6$	62:2	18:1/18:1/26:0; 153%
7888	970.8415	542.6	$C_{61}H_{108}O_7$	O_1 58:5	18:2/18:3/O_1 22:0; 139%	7277	1018.9728	701.1	$C_{65}H_{124}O_6$	62:1	16:0/18:1/28:0; 234%
7887	970.8421	568.9	$C_{61}H_{108}O_7$	O_1 58:5	18:2/22:0/O_1 18:3; 32%	9420	1020.8432	518.8	$C_{61}H_{110}O_{10}$	O_4 58:4	18:1/18:2/O_4 22:1; 41%
7889	970.8430	560.3	$C_{61}H_{108}O_7$	O_1 58:5	18:2/22:1/O_1 18:2; 268%	7914	1026.9050	602.7	$C_{65}H_{116}O_7$	O_1 62:5	18:2/26:0/O_1 18:3; 146%
7891	972.8581	578.4	$C_{61}H_{110}O_7$	O_1 58:4	18:2/20:1/O_1 20:1; 58%	7916	1028.9208	615.8	$C_{65}H_{118}O_7$	O_1 62:4	18:2/26:0/O_1 18:2; 58%
7893	974.8730	593.1	$C_{61}H_{112}O_7$	O_1 58:3	16:0/24:1/O_1 18:2; 70%	7917	1030.9359	630.5	$C_{65}H_{120}O_7$	O_1 62:3	18:2/24:0/O_1 20:1; 71%
7895	976.8889	612.8	$C_{61}H_{114}O_7$	O_1 58:2	18:1/20:1/O_1 20:0; 31%	7278	1036.9271	635.0	$C_{67}H_{118}O_6$	64:6	18:3/18:3/28:0; 151%
7263	978.8486	587.0	$C_{63}H_{108}O_6$	60:7	16:0/18:2/26:5; 39%	7279	1038.9419	650.6	$C_{67}H_{120}O_6$	64:5	18:2/18:3/28:0; 30%
7264	980.8636	602.2	$C_{63}H_{110}O_6$	60:6	18:2/18:3/24:1; 284%	7280	1040.9572	666.5	$C_{67}H_{122}O_6$	64:4	18:2/18:2/28:0; 183%
7896	980.9212	641.5	$C_{61}H_{118}O_7$	O_1 58:0	18:0/20:0/O_1 20:0; 157%	7281	1042.9739	683.2	$C_{67}H_{124}O_6$	64:3	18:1/18:2/28:0; 287%
7265	982.8792	617.0	$C_{63}H_{112}O_6$	60:5	18:2/18:2/24:1; 203%	7282	1044.9885	702.1	$C_{67}H_{126}O_6$	64:2	18:1/18:1/28:0; 175%
8536	984.8208	505.2	$C_{61}H_{106}O_8$	O_2 58:6	22:1/O_1 16:3/O_1 20:2; 31%	8541	1046.9305	586.0	$C_{65}H_{120}O_8$	O_2 62:3	18:2/26:0/O_2 18:1; 187%
7266	984.8948	633.5	$C_{63}H_{114}O_6$	60:4	18:2/18:2/24:0; 193%	7919	1056.9510	632.0	$C_{67}H_{122}O_7$	O_1 64:4	18:2/28:0/O_1 18:2; 86%
7267	986.9106	648.1	$C_{63}H_{116}O_6$	60:3	18:1/18:2/24:0; 250%	7283	1066.9728	665.2	$C_{69}H_{124}O_6$	66:5	18:2/18:2/30:1; 158%
7268	988.9263	664.2	$C_{63}H_{118}O_6$	60:2	16:0/18:2/26:0; 278%	7284	1068.9889	684.6	$C_{69}H_{126}O_6$	66:4	18:2/18:2/30:0; 163%
7897	990.8113	428.9	$C_{63}H_{104}O_7$	O_1 60:9	18:1/18:4/O_1 24:4; 51%	7285	1071.0053	702.6	$C_{69}H_{128}O_6$	66:3	18:1/18:2/30:0; 288%
7269	990.9415	681.4	$C_{63}H_{120}O_6$	60:1	16:0/18:1/26:0; 286%	8544	1100.9789	641.1	$C_{69}H_{126}O_8$	O_2 66:4	18:1/18:3/O_2 30:0; 30%
7900	994.8424	551.2	$C_{63}H_{108}O_7$	O_1 60:7	18:2/18:5/O_1 24:0; 55%	9019	1116.9734	593.1	$C_{69}H_{126}O_9$	O_3 66:4	18:2/O_1 18:2/O_2 30:0; 117%

[a]Highest ranking detected acyl composition and representation in MS/MS spectrum. The sum of intensities of all detected explanatory fragments is expressed in percentage of the base peak intensity (100%).

Eighty intact and oxidized PCs passed all filters. Especially for this lipid class and its lyso form, additional identification of the compositional structure is negatively affected by the dominant head group fragment (*m/z* 184.0733; Fig. 2, D and E). Only nine PCs were structurally annotated. An example is shown in Figure 2D for the precursor *m/z* 830.554 (Supplemental Table S1, Formula_ID = 2322), annotated as protonated O_3 PC 36:4. It was annotated as O_1 18:2/O_2 18:2 with 117% of the base peak intensity. This combination was confirmed by two fragments for the O_1 18:2 acyl chain at *m/z* 297.2394 (protonated O_1 18:2) and 353.2686 (O_1 18:2 FA-glycerol fragment) and by one NL for O_2 18:2 (Δ*m/z* 312.2339).

LysoPCs were validated the same way as PCs, as their head groups are identical. For example, the precursor *m/z* 552.3299 annotated as O_2 lysoPC 18:2 (Supplemental Table S1, Formula_ID = 1850) was validated due to the detection of the head group (Fig. 2E). This also elucidates the structure of the lysoPC, because it contains only the 18:2 FA.

The validation/structure elucidation rules for PEs were analogous to the rules for PCs, but using the PE head group ($C_2H_8NO_4P$). Unlike PCs, PEs were validated mainly by NL of the head group (Δ*m/z* 141.0191). Nineteen PEs passed all filters (Table III), and for 11 of them, acyl compositions were detected. O_1 PE 36:4 (precursor *m/z* 756.518; Supplemental Table S1, Formula_ID = 1440), for example, was found to consist of the FAs 18:2, detected as FA fragment *m/z* 263.2371 and FA-glycerol fragment *m/z* 337.2752, and the complementary FA O_1 18:2 (Fig. 2F). The NL Δ*m/z* 159.0297 often dominated PE MS/MS spectra. The mass corresponds to the NL of the head group $+H_2O$ but was not utilized for the automated annotation. Eleven intact lysoPEs were validated and structure annotated using the rules described for lysoPCs and scanning for the PE head group, but no oxidized lysoPE passed all filters.

PGs were MS/MS validated/structure annotated like PCs/PEs by scanning for the PG head group ($C_3H_9O_6P$) as a fragment or NL. Only neutral head group losses were detected for all 12 validated PGs. For 11 PGs, it was possible to determine the acyl combinations, but none of the fully validated PGs was oxidized. Only two nonoxidized lysoPGs were MS/MS validated and structure annotated following the rules applied for lysoPCs/lysoPEs and scanning for the PG head group as a fragment/NL.

Also, PIs were MS/MS validated and structurally annotated analogous to PCs, PEs, and PGs using the PI head group ($C_6H_{13}O_9P$). Seven PIs were fully validated, and for five of them, the structural composition was determined. We detected no oxidized PI with full validation. We also scanned tentative lysoPIs for the PI head group, but no intact or oxidized lysoPI was MS/MS validated.

GLs are expected to lose their sugar moieties upon collision-induced dissociation. MGDGs were considered as validated when the NL of the galactosyl group ($C_6H_{12}O_6$) was detected with or without additional loss of one or two H_2O molecules and with or without adduct (NH_3). Twenty-seven tentative MGDGs passed all filters, including the MS/MS filter (Table III). Twenty of them also were structurally annotated according to the rules for PCs/PEs, typically yielding more than one combination. Figure 2G displays a typical fragmentation pattern of MGDGs. The precursor *m/z* 830.5983 (Supplemental Table S1, Formula_ID = 8269), annotated as O_2 MGDG 36:3, was validated by a galactosyl $+NH_3$ NL (Δ*m/z* 197.0898) and a galactosyl $-H_2O+NH_3$ NL (Δ*m/z* 179.0811). Three fragments including the base peak could be assigned to the combination of 18:2 (*m/z* 337.274 and 263.2321) and O_2 18:1 (*m/z* 371.280), reflecting 214% of the base peak intensity.

The validation of DGDGs follows the same rules as for MGDGs except that we expected the NL of the digalactosyl moiety $C_{12}H_{24}O_{12}$. Fifty-two DGDGs were MS/MS validated, and 37 of them were structurally annotated (Table III). The example MS/MS spectrum for O_2 DGDG 34:2 (Supplemental Table S1, Formula_ID = 8128) is similar to the MGDG spectrum. Also here, the precursor at *m/z* 966.6361 was validated by two NLs, the digalactosyl moiety $+NH_3$ (Δ*m/z* 377.153) and $-H_2O+NH_3$ (Δ*m/z* 359.1419). The matching acyl composition with highest representation in the spectrum (119%) is 16:0 (*m/z* 239.2390 and 313.2742) and O_2 18:2 (*m/z* 295.2278).

Table III summarizes the MS/MS validation process leading to 624 highly validated lipids with putative acyl compositions for 516 of them. Details regarding the number and abundance of all fully validated lipids at different oxidation levels (compiled to their classes plus FAs) are provided in Table IV.

Warmer Storage Condition Results in the Accumulation of Oxidized Glycerides, FAs, and Membrane Lipid Hydrolysis Products, While the Overall Levels of Intact and Oxidized Membrane Lipids Decrease

Stored cereal seeds lose their viability during storage at ambient temperature (Roberts, 1960). Indirect assays suggest that lipid oxidation is one of the molecular causes associated with the loss in viability (Stewart and Bewley, 1980). This process can be impeded by storing the seeds in the cold and/or anoxic instead of ambient conditions (Harrington, 1963; Groot et al., 2014). We compared the seeds of five wheat accessions harvested in 1998 and stored until 2013 in either ambient or cold conditions. After that, the seeds were shock frozen and stored at −80°C until they were analyzed (Fig. 3). We found massive differences in the oxidation levels of glycerides, FAs, PLs, and GLs. While the levels of nonoxidized TAGs were slightly, although insignificantly, lower in the seeds stored in ambient conditions, the levels of oxidized TAGs were more than twice as high in the ambient versus the cold-stored seeds (Fig. 3A). Both nonoxidized and oxidized DAG levels were approximately twice as high in the ambient compared with the cold-stored seeds (Fig. 3B). The levels of

nonoxidized MAGs were insignificantly higher in the ambient stored seeds, but oxidized MAG levels were elevated significantly (Fig. 3C). The levels of both nonoxidized and oxidized FAs displayed the largest differences observed in this study. They were 4- to 5-fold higher in the ambient compared with the cold-stored seeds (Fig. 3D). Nonoxidized PCs, which are the predominant form of PLs in cellular membranes, were reduced to approximately 50% in the ambient stored seeds, and the levels of oxidized PCs also were slightly, although insignificantly, lower (Fig. 3E). Similar to the PCs, nonoxidized PEs also were reduced to nearly 50% in the ambient stored seeds, but unlike the levels of oxidized PCs, the oxidized PEs were elevated significantly in the ambient stored seeds (Fig. 3F). Also, nonoxidized PGs were reduced by approximately 50% in the ambient stored seeds (Fig. 3G). No putatively annotated oxidized PGs passed all filters. PIs were reduced insignificantly in the ambient stored seeds (Fig. 3H), and oxidized PIs did not pass all filters. The levels of nonoxidized and oxidized lysoPCs were elevated in ambient stored seeds, significant for the oxidized lysoPCs (Fig. 3I). Also, the levels of nonoxidized lysoPEs and lysoPGs were elevated significantly in the ambient stored seeds, but oxidized forms of these two species were not detected after filtering (Fig. 3, J and K). The levels of oxidized MGDGs were reduced to approximately 50% in the ambient stored samples as compared with cold-stored samples, and the levels of nonoxidized MGDGs also were insignificantly lower (Fig. 3L). The levels of both nonoxidized and oxidized DGDGs were reduced to levels below 50% in the ambient compared with the cold-stored seeds (Fig. 3M). The peak height of the seven top abundant TAGs slightly exceeded the linear dynamic range of the detector, which led to a cutoff of the signal due to detector saturation (Fig. 1A; Supplemental Table S1, Median intensity $>$ 100,000,000). We remeasured all samples from 1998 in 1:10 dilution and cross-identified 99 of the 254 annotated (oxy)TAGs (Supplemental Table S8). With respect to relative lipid abundance, the quantitative analysis of the diluted samples led to results fully congruent with the TAG analysis of the undiluted samples (Fig. 3, A and N).

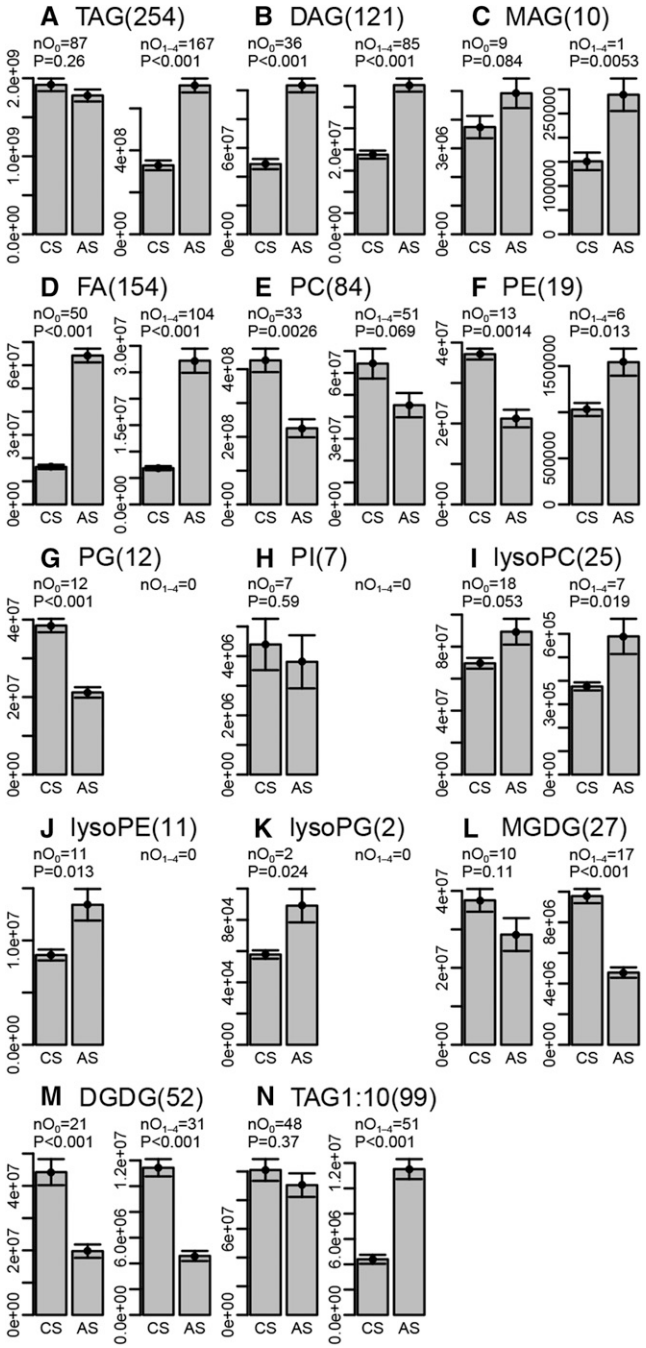

Figure 3. Quantitative analysis of oxidized lipids in long-term stored wheat seeds under ambient and cold conditions. A to M, For each of the 13 detected lipid classes, the number of detected lipid species is given (number in parentheses) and broken down into nonoxidized (nO_0) and oxidized (nO_{1-4}) lipids. Peak areas of all nonoxidized and oxidized lipids were summed up for each of the five seed stocks stored in the cold (CS) or at ambient temperature (AS) from 1998 to 2013. N, TAGs were reanalyzed from 1:10 diluted extracts. Data are means ± SE (n = 5), and significant differences between AS and CS are indicated by ANOVA P values.

DISCUSSION

In plants, lipid oxidation is not a phenomenon restricted to seed aging; instead, it plays a role in many processes, like photooxidative stress (Broin and Rey, 2003), drought-induced leaf damage (Avramova et al., 2017), and metal-induced root damage (Feigl et al., 2015). Also, numerous studies in the fields of microbiology (Imlay, 2013) and medicine (Ames et al., 1993) link lipid oxidation to biological questions of great relevance, like pathogen defense, aging, and cardiovascular diseases. Advances in the comprehensive analysis of oxidized lipids are needed to extend our knowledge in these various research areas.

Previous studies on the systematic quantification and identification of oxidized lipids were conducted mainly using either semitargeted MS/MS (Vu et al., 2012; Spickett and Pitt, 2015) or untargeted high-resolution

MS (Collins et al., 2016), leading to annotations with moderate levels of certainty. By merging accurate mass-derived annotations of a quantitative LC-MS analysis with annotations obtained from a high-resolution MS/MS experiment, we were able to annotate 624 predominantly oxidized lipids in stored wheat seeds with high confidence (Metabolomics Standards Initiative level 2; Sumner et al., 2007). Our method is not restricted to the lipids investigated in this study. It can be expanded to other relevant classes, such as ceramides, by scanning for the sphingoid bases, or DGTS lipids, by scanning for the glycerol-head group fragment (*m/z* 236.150; Yang et al., 2015; Maciel et al., 2016). The whole workflow can be fully translated into negative mode for lipids preferentially forming anions, such as phosphatidic acids (diagnostic lysophosphatidic acid/FA fragments in MS/MS spectrum; http://www.lipidmaps.org/) or sulfoquinovosyldiacylglycerol lipids ($[C_6H_9O_7S]^-$ MS/MS fragment, *m/z* 225.007; Welti et al., 2003).

There is no silver bullet for the comprehensive and reliable identification of compounds like oxidized lipids in an untargeted high-resolution LC-MS data set, as authentic standards often are unavailable. Accurate mass-based annotation performs excellently in metabolite discovery but is prone to yield high numbers of false positives due to isobar molecules with minute mass differences and isomers in biological samples. We annotated lipids with a tolerance of ±1.5 ppm, and more than 92% of all fully validated annotations have an error below 1 ppm. This error is low compared with other recent studies using high-resolution MS (2.5 ppm [Collins et al., 2016], 10 ppm [Li et al., 2017], and 4 mD [Nakabayashi et al., 2017]), and more narrow tolerances lead to fewer false-positive annotations. By the use of isotope, opposite mode, adduct, and retention information, we filtered out erroneously or redundantly annotated lipids and retrieved a list with 1,066 high-confidence annotations. The merits of the filtering procedure are reflected indirectly by the high number of pseudospectra with single analyte annotations (94% of all 1,066 annotations; Table I) and the high number of pseudospectra base peak annotations (86%). But even a mass accuracy of 1 ppm is not regarded as sufficient for unambiguous sum formula identification (Kind and Fiehn, 2006). Using MS/MS spectra, we provided independent proof of identification for 624 of the analytes. Due to their high specificity and inclusion of structural information, the value of (high-resolution) MS/MS spectra in the identification of small molecules is regarded as very high. In addition, the MS/MS spectra provided valuable structural information regarding the acyl composition of 516 of these lipids and the localization of added oxygen atoms in the oxidized lipids. This validation even further increased the number of pseudospectra with single analyte annotations (98%) and pseudospectra base peak annotations (90%). However, in a small number of cases, the filters rejected accurate mass annotations otherwise validated by MS/MS spectra, likely caused by the coisolation of undesired analytes in the MS quadrupole. We followed the suggestion of Hummel et al. (2011) to utilize the systematic shifts in retention time and *m/z* (Fig. 1, B–D) to assess the discovery rate (Supplemental Fig. S4). The mean estimated discovery rates for true positives, true negatives, false positives, and false negatives using O_1 TAGs, O_1 DAGs, PCs, and DGDGs were 82%, 4%, 1%, and 13%. The high proportion of false-negative discoveries was likely caused by missing MS/MS spectra for these precursors (false rendering) or low precursor intensities (less than 10,000 counts, leading to low-quality MS/MS spectra; Supplemental Table S1). From our point of view, the combination of accurate mass annotation, filtering with an acceptable degree of stringency, and MS/MS annotation provides the best and well-balanced solution for highly reliable annotations of (oxidized) lipids.

The heart piece of this study is the massive recording of high-resolution MS/MS spectra and their systematic analysis in order to (1) validate tentative sum formulae assigned by accurate mass and (2) provide structural information with respect to the FA composition of the detected lipids. This required the recording and analysis of MS/MS spectra at high throughput. With the exception of internal/lock-mass calibration and export as net.CDF/mzXML, all in silico steps during recording and data processing/analysis were made in the open-source software environment R using packages and scripts. The computational procedures described in this study can be adopted without creating extra costs for software on a personal computer in less than 24 h, but computational power, preferably a Linux server or at least a workstation, is advisable. The use of SPLs in order to record MS/MS spectra at high throughput is not restricted to Bruker QTOFs. Such or similar lists also can be used with other QTOFs from Agilent, ABSciex, and Waters and ion-trap mass spectrometers (Shimadzu) or orbitrap (Thermo) according to the vendor's information. But also low-resolution instruments like triple-quadrupole mass spectrometers can be used to perform similar analyses. The necessary (Δ) *m/z* of NLs/fragments to program precursor/product ion scan experiments can be retrieved from Supplemental Table S5 and prioritized according to their frequency in the data set (Supplemental Table S6).

In 362 of the 516 MS/MS spectra yielding acyl compositions, several possible acyl combinations were detected. This was often the case for TAGs, and to a lower extent for DAGs and GLs. This might result partially from the above-mentioned coisolation of several lipids with different FA composition in an MS/MS scan, but it is not likely to be the major cause for this observation. As reported by others, lipids with identical sum formulae may occur as multiple isomers in one chromatographic peak (Xu et al., 2009; Li et al., 2014). Lipid isomerism is caused by differences in FA length and distribution along the glycerol backbone, distribution of double bonds and their cis/trans-conformations, and, in the case of oxidized lipids, additional asymmetric centers per oxidation. Hence, single annotations regarding FA composition often are neither meaningful nor

possible. In addition to isomers not separable by the chromatography applied here, we observed isomers that form additional chromatographic peaks. This was the case for very abundant nonoxidized lipids like TAG 54:6, which was found four times but appeared to occur more often in oxidized lipids. TAG 52:4 was found two times in nonoxidized condition, three times with a single additional oxygen, and six times with two additional oxygen molecules (Table V). Then, the numbers drop again to three (three additional oxygen atoms) and two (four additional oxygen atoms) instances. Collins et al. (2016) reported similar observations. Additional isomerism potentially contributing to this phenomenon exists between acyl structures with (1) a hydroxyl group or an epoxy/keto group and a double bond less, (2) two hydroxyl groups or one peroxy group, (3) oxophytodienoic acid or O_1 18:4, and (4) dinor oxophytodienoic acid and O_1 16:4 (Vu et al., 2012). Further knowledge of the fragmentation of different oxylipid isomers in combination with multistage fragmentation experiments (e.g. MS^3) may help to distinguish these variants that are identical in oxidation state and double bond equivalents but different in structure.

We have analyzed 90 wheat seed stocks differing in genotype, harvest year, storage time, and storage conditions and, thus, expected to vary in the degree of lipid oxidation. A total of 259 nonoxidized lipids (Table IV, without FAs) were identified by accurate mass and MS/MS spectra. This is a relatively high number of lipid identifications for analyses where quantitation is conducted (Cajka and Fiehn, 2014). But the number of oxidized lipids (365) is even larger, showing that lipid oxidation is an event leading to relatively large changes in the lipidome. The inclusion of oxidized lipids in lipidomic studies may be helpful or even essential to understand its dynamics. TAG is the principal lipid in wheat seeds (Morrison, 1998), which contain approximately 2% lipids (http://www.fao.org). Assuming that ionization is comparable, 40% of the contents of all TAGs from the 1998 harvest and ambient stored seeds are oxidized (Fig. 3). This implies that the absolute contents of oxidized lipids can be as high as 8 mg g^{-1} dry wheat seed, and probably much higher within the embryo (Bushuk and Rasper, 1994). Further experiments with specimens containing oxidized lipids are needed to confirm the high complexity and magnitude of oxylipidomes in conditions when ROS may occur. Collins et al. (2016) reported that treatment of the diatom *P. tricornutum* with up to 150 μM H_2O_2 for up to 24 h resulted in only marginal differences in the number of oxidized lipids, suggesting that direct chemical oxidation may be a limited model system. Further natural conditions that may result in ROS-dependent lipid oxidation are drought, wounding, O_3, light, salt, metal, and pathogen stress (Pandey et al., 2017). We found clear trends in our data regarding the number and abundance of oxidized lipids. Over all lipid species, we found a quite constant relation of native to oxidized lipids. If there was a large number of annotated TAGs (87), there were also many oxidized TAGs (167), and, vice versa, a small number of lysoPCs (18) coincided with a small number of oxidized lysoPCs (seven). This indicates that a limited and comparable number of oxidized lipids are formed per native lipid. Also, the number and abundance of detectable oxidized lipids within a lipid species decreases with increasing oxidation level. TAGs, PCs, and DGDGs are the terminal products of storage and membrane lipid pathways, and a resting seed does not accumulate more via enzymatic reactions. Also, spontaneous condensation of oxidized constituents to form such a lipid is thermodynamically not favored. In contrast, the pools of DAGs, MAGs, FAs, or lysophospholipids could be formed at least partially by glyceride, PL, or GL hydrolysis during seed aging. The decreasing amount of lipid per added oxygen atom in TAGs, PCs, and DGDGs forms a pattern that resembles a snapshot of ongoing oxidation processes following first- or second-order kinetics. Hence, the observed levels of oxidized lipids are in full agreement with the rate law for a chemical process involving two reactants, lipid molecules and reactive oxygen molecules (or lipid radicals).

Wheat seeds stored in ambient conditions lose their viability over time. When stored in colder conditions, this deterioration process can be slowed down. As shown by our results, the two different storage conditions have a strong effect on lipid oxidation processes (Fig. 3). Consistent with the attribute of the nonoxidized TAGs, PLs, and DGDGs (and also MGDGs) to be a substrate but not a product of conversions in the resting seed, we exclusively observed reductions of contents of these intact lipids under the conditions associated with increased lipid oxidation. One reason for these losses could be oxidation. In fact, this route of reduction appears likely for the intact TAGs, because their reduction coincides with the accumulation of oxidized TAGs. However, oxidation may not be the only cause for the diminishment of intact lipid contents. The reduction of intact membrane lipids, like PCs, MGDGs, and DGDGs, does not coincide with an accumulation of their oxidized counterparts (PEs are an exception here, and for PGs, no oxidized lipid was detectable). Instead, the levels of oxidized membrane lipids are reduced, significant for the GLs. These findings suggest that conversion other than oxidation alone led to losses of the intact PLs and GLs. Hydrolytic cleavage of (oxy)PLs would result in the formation of (oxy)lysophopholipids (elimination of one FA) or (oxy)DAGs (elimination of the head group). The occurrence of such conversions is supported by the observation of increased levels of (oxy)lysophospholipids and (oxy)DAGs in all ambient compared with cold-stored seeds. Further evidence for the hydrolytic cleavage of lipids could be concluded from the massive accumulation of FAs, both intact and oxidized, in the seeds stored in ambient conditions. Our findings clearly show that lipid oxidation processes occur in aged seeds and are enhanced under warm conditions, a treatment associated with reductions in viability (Roberts, 1960; Ellis et al., 1982).

The technical advances introduced in this study enable one to determine lipid oxidation processes at a large scale. Here, we provide a platform-independent workflow for the structural annotation and quantification of relevant oxidized storage and membrane lipids at high confidence by combining accurate mass LC-MS and LC-MS/MS. Our methodology is open for extension to additional lipid classes, particularly at the level of MS/MS validation and composition analysis. As previewed for the increased oxidation of lipids in material prone to oxidative stress, this approach will facilitate the identification of links between oxidative stress and phenological response (e.g. loss of seed viability, pathogen defense, and chronic inflammatory diseases) associated with lipid oxidation in a large number of biological questions.

MATERIALS AND METHODS

Seed Material

Wheat (*Triticum aestivum*) seeds were obtained from the German Federal Genebank hosted at the Leibniz Institute of Plant Genetics and Crop Plant Research in Gatersleben. Seeds were harvested in 1998, 2000, 2001, 2002, 2003, 2004, 2005, 2006, and 2008. Each year, five different genotypes were dried for 4 months at 20°C and 20% relative humidity. At these time points, seeds were dehusked and cleaned, and the stocks were split into two halves. One half was stored in paper bags at 20°C and 50% relative humidity. The other half was stored for another 2 weeks at 20°C and 13% relative humidity, transferred to glasses (Weck) along with silica gel bags, and stored at 0°C until 2008, and from then on at −18°C to comply with contemporary gene bank standards (http://www.fao.org). In 2013, all 90 samples were shock frozen in liquid nitrogen and stored at −80°C until extraction.

Lipid Extraction

Seed material (50 seeds per sample) was homogenized at −80°C using an automatized Cryogrinder (Labman Automation). Lipids were extracted from 25 ± 1 mg using methyl-*tert*-butyl-ether (Biosolve) in randomized order in one batch as described by Giavalisco et al. (2011). The organic supernatant was divided into aliquots and placed into four LC vials (CZT Trott), dried for 3 h in a Speedvac (Martin Christ), crimped under argon, and stored at −80°C in a sealed bag with silica gel until analysis.

LC-MS Analysis

Maximally 24 h prior to injection, sample material was resolubilized in 50 μL of acetonitrile:isopropanol (7:3) and centrifuged for 15 min at 6,200*g*. Then, 2 μL (approximately 160-μg seed weight equivalents) was injected using an MPS2 autosampler (Gerstel) equipped with an ultra-high-pressure injector (Vici Valco). Analytes were separated by a 1290 UHPLC device (Agilent) using a C8 reverse-phase column (150 mm length × 1 mm i.d., 1.7 μm particle o.d.; Waters). The mobile phases consisted of 1% 1 M NH_4Ac and 0.1% acetic acid in water (buffer A) and 1% 1 M NH_4Ac and 0.1% acetic acid in acetonitrile:isopropanol (7:3; buffer B). The flow rate was 200 μL min^{-1}. The gradient was 0.5 min, 55% B; 1.5 min to 65% B; 4 min to 89% B; 4 min to 99% B; 99% B for 5 min; 0.5 min to 55% B; 3.5 min, 55% B. Total run time including equilibration was 19.5 min. Mass spectral analysis was conducted using a Bruker Maxis HD device upgraded with a Maxis II detector (Bruker). MS spectra were recorded at a frequency of 2 Hz from 100 to 1,500 *m/z* with capillary voltage of 4,500 V (positive mode) and 3,000 V (negative mode); nebulizer pressure was set to 1.8 bar, dry gas to 8 L min^{-1}, and dry temperature to 200°C. All spectra of each chromatogram were individually calibrated externally by infusing 20 μL of 10 mM Na-Cluster mix (12.5 mL of water + 12.5 mL of isopropyl alcohol + 50 μL of concentrated formic acid + 250 μL of 1 M NaOH) for the first 4 s of each chromatogram and internally using hexakis(2,2-difluoroethoxy)phosphazene (Apollo Scientific) as lock mass. Calibration and export as net.CDF files was performed using Compass Data Analysis 4.2 (Bruker).

One-to-ten dilutions of all extracts from the 1998 harvested seed stocks were measured under identical conditions in positive mode. *m/z* features were cross-identified to the *m/z* of the peaktable (Supplemental Table S1) generated from the undiluted extracts (retention time match, −9 to −1 s; *m/z* match, ± 2 mD). The *m/z* intensities of all major (oxidized) plant lipids in both dilutions are provided in Supplemental Table S8.

LC-MS/MS Analysis

MS/MS spectra were recorded using the above-mentioned equipment fully upgraded to a Bruker Maxis II. Chromatographic and MS scan settings were identical to the LC-MS settings, but lock-mass infusion/calibration was omitted. An SPL (Supplemental Table S4) containing the retention time point (±1 s; set in the mass spectrometer software) and *m/z* (in a 0.04-D window) of 12,080 potentially monoisotopic features was extracted from the positive-mode LC-MS peaktable (Supplemental Table S1). In auto-MS/MS mode, each MS scan (parent scan) at 2 Hz was followed by an MS/MS scan of the most abundant parent ion on the SPL matching in retention time and *m/z*. The MS/MS scan frequency varied from 2 (intensity < 10,000) to 10 (intensity > 100,000) Hz, with a quadrupole isolation width of ±1 D and a stepped collisional energy of 20 to 50 eV for *m/z* lower than 500 or 24 to 60 eV for *m/z* above 500 *m/z*. Data were externally calibrated and exported as an mzXML file using Compass Data Analysis.

Raw Data Processing

Data processing was conducted on a HP ProLiant DL580 Gen9 CTO (Hewlett Packard) Linux server running RStudio (RStudio). LC-MS raw data in net.CDF format were processed using xcms (Smith et al., 2006) to pick and align peaks in the complete data set (Supplemental Protocol S1). CAMERA (Kuhl et al., 2012) was used to identify *m/z* features from the same analyte by deconvolution and to identify isotopes (Supplemental Protocol S1). Peaks eluting before 20 s or after 720 s were discarded. Peaks found in more than two blank extracts with a median higher than half of the sample median were regarded as background signals and also discarded. Data were seed weight normalized. Each *m/z* feature in the peaktables received a unique mass identifier (Supplemental Tables S1, S2, S4, S6, and S8).

LC-MS/MS raw data in mzXML format were loaded into R using readmzXML (Keller et al., 2005). All 81 LC-MS/MS chromatograms were concatenated into one file containing 30,297 MS/MS spectra. Redundant MS/MS spectra (only the MS/MS spectrum with highest parent ion abundance in the MS scan was kept) and empty MS/MS spectra were removed. Within MS/MS spectra, all *m/z* values greater than the precursor ion, below 0.5% of the base peak intensity, lower than 100 counts, or isotopic and single charged (Kuhl et al., 2012) were removed. All remaining 8,957 nonredundant MS/MS spectra (Supplemental Fig. S2) were assigned to the features in the LC-MS peaktable (Supplemental Table S1) by matching the trigger precursor *m/z* of the MS scans to the *m/z* features in the LC-MS peaktable using retention time (−3 to +1 s) and *m/z* (±5 mD).

Accession Numbers

The processed 8,957 MS/MS spectra are available online at MassIVE (ftp://massive.ucsd.edu/MSV000081200) and at the Global Natural Products Social Molecular Networking site (GNPS; ID MSV000081200).

Supplemental Data

The following supplemental materials are available.

Supplemental Figure S1. *m/z* correction.

Supplemental Figure S2. Positive-mode MS/MS spectra.

Supplemental Figure S3. LIPID MAPS MS/MS spectra.

Supplemental Figure S4. Discovery rate estimation.

Supplemental Table S1. Positive-mode peaktable.

Supplemental Table S2. Negative-mode peaktable.

Supplemental Table S3. Oxylipid target list for accurate mass annotation.

Supplemental Table S4. Scheduled precursor list for LC-MS/MS analysis.

Supplemental Table S5. Fragment/NL library.

Supplemental Table S6. Fragment/NL annotation.

Supplemental Table S7. Lipid structure library.

Supplemental Table S8. TAGs of 1:10 diluted extracts.

Supplemental Protocol S1. xcms/CAMERA settings.

ACKNOWLEDGMENTS

We thank Andrea Apelt for excellent technical assistance; the seed material was provided by Dr. Andreas Boerner; we acknowledge the services of MassIVE and GNPS to provide and process the MS/MS spectra produced in this work.

Received April 5, 2017; accepted August 5, 2017; published August 11, 2017.

LITERATURE CITED

Ames BN, Shigenaga MK, Hagen TM (1993) Oxidants, antioxidants, and the degenerative diseases of aging. Proc Natl Acad Sci USA **90:** 7915–7922

Anesi A, Guella G (2015) A fast liquid chromatography-mass spectrometry methodology for membrane lipid profiling through hydrophilic interaction liquid chromatography. J Chromatogr A **1384:** 44–52

Avramova V, AbdElgawad H, Vasileva I, Petrova AS, Holek A, Mariën J, Asard H, Beemster GT (2017) High antioxidant activity facilitates maintenance of cell division in leaves of drought tolerant maize hybrids. Front Plant Sci **8:** 84

Bandu R, Mok HJ, Kim KP (2016) Phospholipids as cancer biomarkers: mass spectrometry-based analysis. Mass Spectrom Rev

Berlett BS, Stadtman ER (1997) Protein oxidation in aging, disease, and oxidative stress. J Biol Chem **272:** 20313–20316

Birtic S, Ksas B, Genty B, Mueller MJ, Triantaphylidès C, Havaux M (2011) Using spontaneous photon emission to image lipid oxidation patterns in plant tissues. Plant J **67:** 1103–1115

Broin M, Rey P (2003) Potato plants lacking the CDSP32 plastidic thioredoxin exhibit overoxidation of the BAS1 2-cysteine peroxiredoxin and increased lipid peroxidation in thylakoids under photooxidative stress. Plant Physiol **132:** 1335–1343

Buseman CM, Tamura P, Sparks AA, Baughman EJ, Maatta S, Zhao J, Roth MR, Esch SW, Shah J, Williams TD, et al (2006) Wounding stimulates the accumulation of glycerolipids containing oxophytodienoic acid and dinor-oxophytodienoic acid in Arabidopsis leaves. Plant Physiol **142:** 28–39

Bushuk W, Rasper VF (1994) Wheat: Production, Properties and Quality. Chapman & Hall, London

Byrdwell WC, Neff WE (2002) Dual parallel electrospray ionization and atmospheric pressure chemical ionization mass spectrometry (MS), MS/MS and MS/MS/MS for the analysis of triacylglycerols and triacylglycerol oxidation products. Rapid Commun Mass Spectrom **16:** 300–319

Cajka T, Fiehn O (2014) Comprehensive analysis of lipids in biological systems by liquid chromatography-mass spectrometry. Trends Analyt Chem **61:** 192–206

Cao M, Fraser K, Huege J, Featonby T, Rasmussen S, Jones C (2015) Predicting retention time in hydrophilic interaction liquid chromatography mass spectrometry and its use for peak annotation in metabolomics. Metabolomics **11:** 696–706

Chen HH, Chu P, Zhou YL, Ding Y, Li Y, Liu J, Jiang LW, Huang SZ (2016) Ectopic expression of NnPER1, a *Nelumbo nucifera* 1-cysteine peroxiredoxin antioxidant, enhances seed longevity and stress tolerance in Arabidopsis. Plant J **88:** 608–619

Chu P, Chen H, Zhou Y, Li Y, Ding Y, Jiang L, Tsang EWT, Wu K, Huang S (2012) Proteomic and functional analyses of *Nelumbo nucifera* annexins involved in seed thermotolerance and germination vigor. Planta **235:** 1271–1288

Collins JR, Edwards BR, Fredricks HF, Van Mooy BA (2016) LOBSTAHS: an adduct-based lipidomics strategy for discovery and identification of oxidative stress biomarkers. Anal Chem **88:** 7154–7162

Colville L, Bradley EL, Lloyd AS, Pritchard HW, Castle L, Kranner I (2012) Volatile fingerprints of seeds of four species indicate the involvement of alcoholic fermentation, lipid peroxidation, and Maillard reactions in seed deterioration during ageing and desiccation stress. J Exp Bot **63:** 6519–6530

Coyle JT, Puttfarcken P (1993) Oxidative stress, glutamate, and neurodegenerative disorders. Science **262:** 689–695

Ejsing CS, Sampaio JL, Surendranath V, Duchoslav E, Ekroos K, Klemm RW, Simons K, Shevchenko A (2009) Global analysis of the yeast lipidome by quantitative shotgun mass spectrometry. Proc Natl Acad Sci USA **106:** 2136–2141

Ellis RH, Osei-Bonsu K, Roberts EH (1982) The influence of genotype, temperature and moisture on seed longevity in chickpea, cowpea and soya bean. Ann Bot (Lond) **50:** 69–82

Feigl G, Lehotai N, Molnár Á, Ördög A, Rodríguez-Ruiz M, Palma JM, Corpas FJ, Erdei L, Kolbert Z (2015) Zinc induces distinct changes in the metabolism of reactive oxygen and nitrogen species (ROS and RNS) in the roots of two Brassica species with different sensitivity to zinc stress. Ann Bot (Lond) **116:** 613–625

Giavalisco P, Li Y, Matthes A, Eckhardt A, Hubberten HM, Hesse H, Segu S, Hummel J, Köhl K, Willmitzer L (2011) Elemental formula annotation of polar and lipophilic metabolites using (13) C, (15) N and (34) S isotope labelling, in combination with high-resolution mass spectrometry. Plant J **68:** 364–376

Gilroy S, Białasek M, Suzuki N, Górecka M, Devireddy AR, Karpiński S, Mittler R (2016) ROS, calcium, and electric signals: key mediators of rapid systemic signaling in plants. Plant Physiol **171:** 1606–1615

Giugliano D, Ceriello A, Paolisso G (1996) Oxidative stress and diabetic vascular complications. Diabetes Care **19:** 257–267

Goel A, Sheoran IS (2003) Lipid peroxidation and peroxide-scavenging enzymes in cotton seeds under natural ageing. Biol Plant **46:** 429–434

Groot SPC, de Groot L, Kodde J, van Treuren R (2014) Prolonging the longevity of ex situ conserved seeds by storage under anoxia. Plant Genet Resour **13:** 18–26

Hagiwara T, Saito S, Ujiie Y, Imai K, Kakuta M, Kadota K, Terada T, Sumikoshi K, Shimizu K, Nishi T (2010) HPLC retention time prediction for metabolome analysi. Bioinformation **5:** 255–258

Harrington JF (1963) Practical instructions and advice on seed storage. Proceedings of the International Seed Testing Association **28:** 989–994

Herzog R, Schwudke D, Shevchenko A (2002) LipidXplorer: software for quantitative shotgun lipidomics compatible with multiple mass spectrometry platforms. Curr Protoc Bioinformatics **14:**14.12:14.12.1–14.12.30

Hui SP, Chiba H, Jin S, Nagasaka H, Kurosawa T (2010) Analyses for phosphatidylcholine hydroperoxides by LC/MS. J Chromatogr B Analyt Technol Biomed Life Sci **878:** 1677–1682

Hummel J, Segu S, Li Y, Irgang S, Jueppner J, Giavalisco P (2011) Ultra performance liquid chromatography and high resolution mass spectrometry for the analysis of plant lipids. Front Plant Sci **2:** 54

Imlay JA (2013) The molecular mechanisms and physiological consequences of oxidative stress: lessons from a model bacterium. Nat Rev Microbiol **11:** 443–454

Ivanova PT, Milne SB, Myers DS, Brown HA (2009) Lipidomics: a mass spectrometry based systems level analysis of cellular lipids. Curr Opin Chem Biol **13:** 526–531

Keller A, Eng J, Zhang N, Li XJ, Aebersold R (2005) A uniform proteomics MS/MS analysis platform utilizing open XML file formats. Mol Syst Biol **1:** 0017

Kind T, Fiehn O (2006) Metabolomic database annotations via query of elemental compositions: mass accuracy is insufficient even at less than 1 ppm. BMC Bioinformatics **7:** 234

Kind T, Liu KH, Lee DY, DeFelice B, Meissen JK, Fiehn O (2013) LipidBlast in silico tandem mass spectrometry database for lipid identification. Nat Methods **10:** 755–758

Koelmel JP, Kroeger NM, Gill EL, Ulmer CZ, Bowden JA, Patterson RE, Yost RA, Garrett TJ (2017) Expanding lipidome coverage using LC-MS/MS data-dependent acquisition with automated exclusion list generation. J Am Soc Mass Spectrom **28:** 908–917

Kuhl C, Tautenhahn R, Böttcher C, Larson TR, Neumann S (2012) CAMERA: an integrated strategy for compound spectra extraction and annotation of liquid chromatography/mass spectrometry data sets. Anal Chem **84:** 283–289

Lee YP, Baek KH, Lee HS, Kwak SS, Bang JW, Kwon SY (2010) Tobacco seeds simultaneously over-expressing Cu/Zn-superoxide dismutase and ascorbate peroxidase display enhanced seed longevity and germination rates under stress conditions. J Exp Bot **61:** 2499–2506

Li M, Butka E, Wang X (2014) Comprehensive quantification of triacylglycerols in soybean seeds by electrospray ionization mass spectrometry with multiple neutral loss scans. Sci Rep **4:** 6581

Li Q, Bozek K, Xu C, Guo Y, Sun J, Pääbo S, Sherwood CC, Hof PR, Ely JJ, Li Y, et al (2017) Changes in lipidome composition during brain development in humans, chimpanzees, and macaque monkeys. Mol Biol Evol **34:** 1155–1166

Lommen A, Gerssen A, Oosterink JE, Kools HJ, Ruiz-Aracama A, Peters RJ, Mol HG (2011) Ultra-fast searching assists in evaluating sub-ppm mass accuracy enhancement in U-HPLC/Orbitrap MS data. Metabolomics **7:** 15–24

Loos M, Gerber C, Corona F, Hollender J, Singer H (2015) Accelerated isotope fine structure calculation using pruned transition trees. Anal Chem **87:** 5738–5744

Maciel E, Costa Leal M, Lillebø AI, Domingues P, Domingues MR, Calado R (2016) Bioprospecting of marine macrophytes using MS-based lipidomics as a new approach. Mar Drugs **14:** 49

Manicke NE, Wiseman JM, Ifa DR, Cooks RG (2008) Desorption electrospray ionization (DESI) mass spectrometry and tandem mass spectrometry (MS/MS) of phospholipids and sphingolipids: ionization, adduct formation, and fragmentation. J Am Soc Mass Spectrom **19:** 531–543

Mignolet-Spruyt L, Xu E, Idänheimo N, Hoeberichts FA, Mühlenbock P, Brosché M, Van Breusegem F, Kangasjärvi J (2016) Spreading the news: subcellular and organellar reactive oxygen species production and signalling. J Exp Bot **67:** 3831–3844

Mihaleva VV, Vorst O, Maliepaard C, Verhoeven HA, de Vos RCH, Hall RD, van Ham RCHJ (2008) Accurate mass error correction in liquid chromatography time-of-flight mass spectrometry based metabolomics. Metabolomics **4:** 171–182

Morita M, Naito Y, Yoshikawa T, Niki E (2016) Rapid assessment of singlet oxygen-induced plasma lipid oxidation and its inhibition by antioxidants with diphenyl-1-pyrenylphosphine (DPPP). Anal Bioanal Chem **408:** 265–270

Morrison WR (1998) Wheat lipid composition. Cereal Chem **55:** 548–558

Murphy RC, Axelsen PH (2011) Mass spectrometric analysis of long-chain lipids. Mass Spectrom Rev **30:** 579–599

Nakabayashi R, Hashimoto K, Toyooka K, Saito K (2017) Top-down metabolomic approaches for nitrogen-containing metabolites. Anal Chem **89:** 2698–2703

Pandey S, Fartyal D, Agarwal A, Shukla T, James D, Kaul T, Negi YK, Arora S, Reddy MK (2017) Abiotic stress tolerance in plants: myriad roles of ascorbate peroxidase. Front Plant Sci **8:** 581

Pant BD, Burgos A, Pant P, Cuadros-Inostroza A, Willmitzer L, Scheible WR (2015) The transcription factor PHR1 regulates lipid remodeling and triacylglycerol accumulation in Arabidopsis thaliana during phosphorus starvation. J Exp Bot **66:** 1907–1918

Perluigi M, Coccia R, Butterfield DA (2012) 4-Hydroxy-2-nonenal, a reactive product of lipid peroxidation, and neurodegenerative diseases: a toxic combination illuminated by redox proteomics studies. Antioxid Redox Signal **17:** 1590–1609

Ravandi A, Leibundgut G, Hung MY, Patel M, Hutchins PM, Murphy RC, Prasad A, Mahmud E, Miller YI, Dennis EA, et al (2014) Release and capture of bioactive oxidized phospholipids and oxidized cholesteryl esters during percutaneous coronary and peripheral arterial interventions in humans. J Am Coll Cardiol **63:** 1961–1971

Roberts EH (1960) The viability of cereal seed in relation to temperature and moisture: with eight figures in the text. Ann Bot (Lond) **24:** 12–31

Schwudke D, Oegema J, Burton L, Entchev E, Hannich JT, Ejsing CS, Kurzchalia T, Shevchenko A (2006) Lipid profiling by multiple precursor and neutral loss scanning driven by the data-dependent acquisition. Anal Chem **78:** 585–595

Schwudke D, Schuhmann K, Herzog R, Bornstein SR, Shevchenko A (2011) Shotgun lipidomics on high resolution mass spectrometers. Cold Spring Harb Perspect Biol **3:** a004614

Smith CA, Want EJ, O'Maille G, Abagyan R, Siuzdak G (2006) XCMS: processing mass spectrometry data for metabolite profiling using nonlinear peak alignment, matching, and identification. Anal Chem **78:** 779–787

Sohal RS, Mockett RJ, Orr WC (2002) Mechanisms of aging: an appraisal of the oxidative stress hypothesis. Free Radic Biol Med **33:** 575–586

Sohal RS, Weindruch R (1996) Oxidative stress, caloric restriction, and aging. Science **273:** 59–63

Spickett CM (2013) The lipid peroxidation product 4-hydroxy-2-nonenal: advances in chemistry and analysis. Redox Biol **1:** 145–152

Spickett CM, Pitt AR (2015) Oxidative lipidomics coming of age: advances in analysis of oxidized phospholipids in physiology and pathology. Antioxid Redox Signal **22:** 1646–1666

Stewart RR, Bewley JD (1980) Lipid peroxidation associated with accelerated aging of soybean axes. Plant Physiol **65:** 245–248

Sumner LW, Amberg A, Barrett D, Beale MH, Beger R, Daykin CA, Fan TW, Fiehn O, Goodacre R, Griffin JL, et al (2007) Proposed minimum reporting standards for chemical analysis: Chemical Analysis Working Group (CAWG) Metabolomics Standards Initiative (MSI). Metabolomics **3:** 211–221

Szymanski J, Brotman Y, Willmitzer L, Cuadros-Inostroza Á (2014) Linking gene expression and membrane lipid composition of *Arabidopsis*. Plant Cell **26:** 915–928

Taguchi R, Houjou T, Nakanishi H, Yamazaki T, Ishida M, Imagawa M, Shimizu T (2005) Focused lipidomics by tandem mass spectrometry. J Chromatogr B Analyt Technol Biomed Life Sci **823:** 26–36

Thiele H, McLeod G, Niemitz M, Kühn T (2011) Structure verification of small molecules using mass spectrometry and NMR spectroscopy. Monatshefte fur Chemie Chemical Monthly **142:** 717–730

Vu HS, Tamura P, Galeva NA, Chaturvedi R, Roth MR, Williams TD, Wang X, Shah J, Welti R (2012) Direct infusion mass spectrometry of oxylipin-containing Arabidopsis membrane lipids reveals varied patterns in different stress responses. Plant Physiol **158:** 324–339

Welti R, Wang X, Williams TD (2003) Electrospray ionization tandem mass spectrometry scan modes for plant chloroplast lipids. Anal Biochem **314:** 149–152

Xu F, Zou L, Lin Q, Ong CN (2009) Use of liquid chromatography/tandem mass spectrometry and online databases for identification of phosphocholines and lysophosphatidylcholines in human red blood cells. Rapid Commun Mass Spectrom **23:** 3243–3254

Yakes FM, Van Houten B (1997) Mitochondrial DNA damage is more extensive and persists longer than nuclear DNA damage in human cells following oxidative stress. Proc Natl Acad Sci USA **94:** 514–519

Yang D, Song D, Kind T, Ma Y, Hoefkens J, Fiehn O (2015) Lipidomic analysis of *Chlamydomonas reinhardtii* under nitrogen and sulfur deprivation. PLoS ONE **10:** e0137948

Zeb A (2012) Triacylglycerols composition, oxidation and oxidation compounds in camellia oil using liquid chromatography-mass spectrometry. Chem Phys Lipids **165:** 608–614